Article

Neuron

Neonatal *Tbr1* Dosage Controls Cortical Layer 6 Connectivity

Highlights

- *Tbr1* specifies layer 6 dendritic patterning and cell-intrinsic physiology
- *Tbr1* promotes synapse numbers through *Wnt7b*
- *Tbr1* heterozygotes provide insight into ASD pathophysiology
- TBR1 directly regulates transcriptional circuits that controls ASD risk genes

Authors

Siavash Fazel Darbandi, Sarah E. Robinson Schwartz, Qihao Qi, ..., Matthew W. State, Vikaas S. Sohal, John L.R. Rubenstein

Correspondence

matthew.state@ucsf.edu (M.W.S.), john.rubenstein@ucsf.edu (J.L.R.R.)

In Brief

TBR1 directly regulates transcriptional circuits in heterozygous mutant mice that specify layer 6 identity and synapse number. As *TBR1* is an ASD risk gene, our results provide insights into mechanisms that underlie ASD pathophysiology.

Fazel Darbandi et al., 2018, Neuron *100*, 1–15
November 21, 2018 © 2018 Elsevier Inc.
https://doi.org/10.1016/j.neuron.2018.09.027

CellPress

Please cite this article in press as: Fazel Darbandi et al., Neonatal *Tbr1* Dosage Controls Cortical Layer 6 Connectivity, Neuron (2018), https://doi.org/10.1016/j.neuron.2018.09.027

Neuron
Article

Neonatal *Tbr1* Dosage Controls Cortical Layer 6 Connectivity

Siavash Fazel Darbandi,[1,5] Sarah E. Robinson Schwartz,[5] Qihao Qi,[4,5] Rinaldo Catta-Preta,[3] Emily Ling-Lin Pai,[1] Jeffrey D. Mandell,[4] Amanda Everitt,[4] Anna Rubin,[1,5] Rebecca A. Krasnoff,[4] Sol Katzman,[2] David Tastad,[2] Alex S. Nord,[3] A. Jeremy Willsey,[4,5,7] Bin Chen,[2] Matthew W. State,[5,7,*] Vikaas S. Sohal,[5,6] and John L.R. Rubenstein[1,5,8,*]
[1]Nina Ireland Laboratory of Developmental Neurobiology, Department of Psychiatry, and Weill Institute for Neurosciences, University of California, San Francisco, San Francisco, CA 94143, USA
[2]Department of Molecular, Cell, and Developmental Biology, University of California, Santa Cruz, Santa Cruz, CA 95064, USA
[3]Department of Neurobiology, Physiology, and Behavior and Department of Psychiatry and Behavioral Sciences, Center for Neuroscience, University of California, Davis, Davis, CA 95618, USA
[4]Institute for Neurodegenerative Diseases, UCSF Weill Institute for Neurosciences, University of California, San Francisco, San Francisco, CA 94143, USA
[5]Department of Psychiatry, Weill Institute for Neurosciences, University of California, San Francisco, San Francisco, CA 94143, USA
[6]Kavli Institute for Fundamental Neuroscience and Sloan-Swartz Center for Theoretical Neurobiology, University of California, San Francisco, San Francisco, CA 94143, USA
[7]Quantitative Biosciences Institute (QBI), University of California, San Francisco, San Francisco, CA 94143, USA
[8]Lead Contact
*Correspondence: matthew.state@ucsf.edu (M.W.S.), john.rubenstein@ucsf.edu (J.L.R.R.)
https://doi.org/10.1016/j.neuron.2018.09.027

SUMMARY

An understanding of how heterozygous loss-of-function mutations in autism spectrum disorder (ASD) risk genes, such as TBR1, contribute to ASD remains elusive. Conditional *Tbr1* deletion during late mouse gestation in cortical layer 6 neurons (*Tbr1*^{layer6} mutants) provides novel insights into its function, including dendritic patterning, synaptogenesis, and cell-intrinsic physiology. These phenotypes occur in heterozygotes, providing insights into mechanisms that may underlie ASD pathophysiology. Restoring expression of *Wnt7b* largely rescues the synaptic deficit in *Tbr1*^{layer6} mutant neurons. Furthermore, *Tbr1*^{layer6} heterozygotes have increased anxiety-like behavior, a phenotype seen ASD. Integrating TBR1 chromatin immunoprecipitation sequencing (ChIP-seq) and RNA sequencing (RNA-seq) data from layer 6 neurons and activity of TBR1-bound candidate enhancers provides evidence for how TBR1 regulates layer 6 properties. Moreover, several putative TBR1 targets are ASD risk genes, placing TBR1 in a central position both for ASD risk and for regulating transcriptional circuits that control multiple steps in layer 6 development essential for the assembly of neural circuits.

INTRODUCTION

Autism spectrum disorder (ASD) is defined by impairments in reciprocal social interaction, often accompanied by abnormalities in language development as well as repetitive behaviors and/or restricted interests. Recent progress in detection and analysis of rare variants in ASD has led to reliable and systematic gene discovery and revealed a group of 28 genes with the strongest statistical evidence for association with ASD risk (defined by false discovery rate [FDR] < 0.01) (Sanders et al., 2015). These highest-confidence ASD (hcASD) genes encode various groups of proteins, including transcription factors (*Tbr1* and *Tcf7l2;* mouse orthologs listed), synaptic genes (*Scn2a1* and *Syngap1*), and chromatin remodelers (*Chd8* and *Arid1b*) (Sanders et al., 2015). Furthermore, among the top 65 ASD genes (FDR < 0.1) (Sanders et al., 2015), *Tbr1*, *Bcl11a*, and *Foxp1* transcription factors (TFs) are implicated in mouse cortical development. Systems analyses of ASD genes revealed that there is a convergence of ASD-risk gene expression in mid-fetal prefrontal cortex concentrated in the excitatory neurons of deep cortical layers 5 and 6 (Willsey et al., 2013). However, an actionable understanding of how large-effect, heterozygous loss-of-function mutations in risk genes are contributing to the pathophysiology of ASD remains elusive. Thus, we explored how conditional deletion of mouse *Tbr1* in cortical layer 6, at a developmental interval roughly equivalent to human mid-fetal stages, alters neuronal identity and function in homozygous and heterozygous mutants.

T-brain-1 (*Tbr1*), a T-box TF, has a central role in early cortical development. During neurodevelopment and in adulthood, *Tbr1* is expressed in the excitatory neurons of the neocortex (subplate, layer 6, rostral layer 5, and layers 2/3), hippocampus, entorhinal cortex, pallial amygdala, piriform cortex, and olfactory bulb and Cajal-Retzius (CR) neurons (Hevner et al., 2001, 2003). The encoded protein regulates development of early-born pallial projection neurons, including CR cells and subplate and layer 6 projection neurons (Bedogni et al., 2010; Hevner et al., 2001; Bulfone et al., 1995). *Tbr1* constitutive null (*Tbr1*$^{constitutive\ null}$) mouse showed defects in layer 6 corticothalamic neurons (Bedogni et al., 2010; Bulfone et al., 1998). *Tbr1* promotes layer 6 identity by repressing *Fezf2* and *Bcl11b,* TFs that

control layer 5 fate (McKenna et al., 2011; Han et al., 2011). Moreover, *Tbr1*$^{constitutive\ heterozygous}$ mice have abnormal inter- and intra-amygdalar axonal projections (Chuang et al., 2015; Huang et al., 2014). Lastly, TBR1 binds to the *Grin2b* promoter and promotes *Grin2b* expression upon neuronal activation (Chuang et al., 2014). However, many important aspects of *Tbr1* function have yet to be clarified, including elucidating its role in early post-natal mouse brain development, characterizing the composition of *Tbr1*-regulated gene networks and their *cis*-regulatory elements, and understanding the consequence of *Tbr1* heterozygosity on neocortical development and function.

Here, we have used conditional mutagenesis to define early postnatal functions of *Tbr1* in layer 6 cortical projection neurons by creating a viable *Tbr1*^{layer6} mutant. The *Tbr1*^{layer6} homozygous mutant neurons take on a hybrid layer 5 and layer 6 identity based on their gene expression profile, dendritic pattern, and physiology. *Tbr1* promotes expression of layer 6 markers (*Foxp2*, *Nr4a2*, *Tle4*, and *Wnt7b*) and represses expression of layer 5 identity regulators (*Fezf2* and *Bcl11b*). *Tbr1*^{layer6} homozygous mutants also have altered RNA levels of *Scn2a1* and *Grin2b* (orthologs of hcASD genes), as well as of *Bcl11a*, *Foxp1*, *Nuak1*, and *Wnt7b* (orthologs of probable ASD genes [FDR < 0.3]) (Sanders et al., 2015).

TBR1 and other ASD genes have been identified based on heterozygous rare variants observed in cases, and therefore, it is of interest to characterize the phenotype of *Tbr1*^{layer6} heterozygotes. In these animals, we observe that *Wnt7b* and *Bcl11a* expression are reduced in layer 6, whereas *Fezf2* is ectopically expressed in layer 6, providing insight into perturbations that may occur in ASD patients. Furthermore, neurons from both the *Tbr1*^{layer6} heterozygous and homozygous mice have reduced excitatory and inhibitory synaptic density as well as spontaneous excitatory postsynaptic currents (EPSCs) and inhibitory postsynaptic currents (IPSCs). Restoring expression of *Wnt7b* (a direct TBR1 target) largely rescues the synaptic deficit phenotype in *Tbr1*^{layer6} heterozygous and homozygous neurons *in vitro* and *in vivo*. Collectively, we propose that these phenotypes, and the *Tbr1*-regulated gene regulatory networks, shed light on how *Tbr1* loss-of-function mutation disrupt neural function and connectivity. Importantly, we find that *Tbr1*^{layer6} heterozygous mutants have reduced synapse numbers and functions, mechanisms that have been strongly implicated in ASD pathogenesis (De Rubeis et al., 2014). Thus, our analysis adds fundamentally to understanding of how a single TF regulates a temporal sequence of steps in cortical development that have implications for understanding complex human social behaviors.

RESULTS

Tbr1 Conditional Mutant Allele

To investigate the functions of *Tbr1* in specific subtypes of cortical neurons at later stages of development, we generated a *Tbr1* conditional mutant (*Tbr1*^{flox}) allele by inserting *loxP* sites into introns 1 and 3 (Figure S1A). We validated that recombination using *β-actin-Cre* eliminated expression of TBR1 protein and RNA encoded by the deleted exons (Figures S1C and S1E). Thus, it is likely to be a null allele, even though a truncated RNA continues to be expressed (Figure S1D). Upon recombination with *Ntsr1-cre*, TBR1 protein levels were reduced by ~90% in layer 6 and subplate at P0 (Figure S1F).

Tbr1 Maintains Layer 6 Identity in the Postnatal Cortex

To restrict *Tbr1* perturbation to layer 6 and subplate, we deleted *Tbr1* 5–6 days after *Tbr1* expression begins using neurotensin receptor 1-Cre mice (*Ntsr1-cre*). We refer to these mice as *Tbr1*^{layer6} mutants. *Ntsr1-cre* expression begins in layer 6 at approximately embryonic day 16.5 (E16.5) (data not shown). To identify putative *Tbr1* regulatory targets in layer 6 and subplate, we compared gene expression profiles using fluorescence-activated cell sorting (FACS) in layer 6 neurons from mutant and wild-type mice. More specifically, we generated RNA sequencing (RNA-seq) data from layer 6 neurons isolated from postnatal day 5 (P5) *Tbr1*$^{wild\text{-}type}$, *Tbr1*^{layer6} heterozygous and homozygous mutant somatosensory cortex (SSCx). We identified 178 differentially expressed (DEX) genes in *Tbr1*^{layer6} homozygous mutants (false discovery rate $\leq$ 0.05) (Figure 1A; Tables S1 and S2). However, transcriptomic analysis of *Tbr1*^{layer6} heterozygous mutants did not reveal conclusive evidence for changes in RNA levels (data not shown).

We observed increased expression of several regulators of layer 5 identity in layer 6 neurons isolated from *Tbr1*^{layer6} homozygous mutants, including *Fezf2* and *Bcl11b*. Additionally we observed decreased expression of RNAs encoding regulators and/or markers of layer 6 identity, including *Foxp2*, *Nr4a2*, *Tle4*, and *Wnt7b*. Together, this suggests that layer 6 neurons from P5 *Tbr1*^{layer6} mutants have changed fate to a layer-5-like identity.

To better understand the consequence of these transcriptomic changes on the identity of the layer 6 mutant neurons, we identified genes that distinguish layer 5 and layer 6 pyramidal neurons in P5 wild-type mice. To accomplish this, we generated RNA-seq data from FACS-purified layer 5 neurons and compared with RNA-seq data from FACS-purified layer 6 neurons. We identified 35 DEX genes that distinguish layer 6 and layer 5 wild-type neurons (denoted as layer 5/6 DEX genes; Figure 1B). Next, we compared the layer 5/6 DEX genes with the genes dysregulated in layer 6 neurons from *Tbr1*^{layer6} null mice. With respect to genes that mark wild-type layer 5 (red genes; Figure 1B), we observed eight genes with increased expression in the *Tbr1*^{layer6} mutants ($p < 0.05$). Moreover, with respect to genes that mark wild-type layer 6 (blue genes in Figure 1B), we observed 13 with reduced expression in the *Tbr1*^{layer6} mutants ($p < 0.05$; Figure 1B; Table S3). On the contrary, the analysis identified 14 of the layer 5 and layer 6 marker genes, whose expression did not significantly change in the *Tbr1*^{layer6} mutants (Figure 1B; Table S3). This suggests that *Tbr1*^{layer6} mutant neurons have a hybrid identity, with transcriptomic properties of both layer 5 and layer 6 pyramidal neurons.

In situ hybridization confirmed some of these results at P3 (Figure 2; Table S4). Regulators and/or markers of layer 6 identity were downregulated in *Tbr1*^{layer6} homozygous (e.g., *Foxp2*, *Tle4*, *Nr4a2*, and *Wnt7b*) and *Tbr1*^{layer6} heterozygous mutants (e.g., *Wnt7b*, *Bcl11a*; Figure 2), whereas the expression of *Fezf2,* a regulator of layer 5 identity, was upregulated in layer 6 mutant neurons (Figure 2). Overall, our RNA expression data

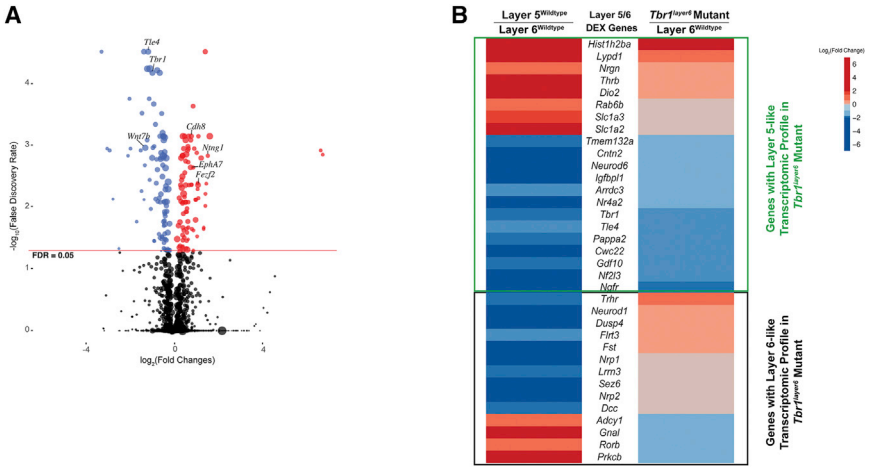

Figure 1. *Tbr1* Transcriptional Regulation in the Neonatal Cortex

(A) Volcano plot of genes upregulated (red) and downregulated (blue) in FACS purified layer 6 neurons from P5 $Tbr1^{layer6}$ homozygous mutant SSCx. Black dots represent the genes that did not reach statistical significance (adjusted p value > 0.05). The size of each point represents the difference in the median gene expression between $Tbr1^{wild\text{-}type}$ and $Tbr1^{layer6}$ mutant (large dots mean large differences).

(B) P5 transcriptomic comparison of DEX genes between layer $5^{wild\text{-}type}$ versus layer $6^{wild\text{-}type}$ and $Tbr1^{layer6}$ homozygotes versus $layer6^{wild\text{-}type}$. With respect to genes that mark wild-type layer 5 (red genes), we observed eight genes with increased expression in the $Tbr1^{layer6}$ mutants ($p < 0.05$). With respect to genes that mark wild-type layer 6 (blue genes), we observed 13 with reduced expression in the $Tbr1^{layer6}$ mutants ($p < 0.05$). However, there were 14 of the layer 5 and layer 6 marker genes whose expression did not significantly change in the $Tbr1^{layer6}$ mutants. Genes with layer-5-like transcriptome profile (green box) and layer-6-like expression profile (black box) are indicated.

See also Figure S1 and Tables S1, S2, and S3.

(RNA-seq and ISH) demonstrates that late gestational/neonatal *Tbr1* expression is essential to maintain layer 6 identity.

Tbr1 Directly Regulates the Transcription of Genes that Control Layer 6 Identity

To determine the regions of the genome that TBR1 interacts with, and whether the changes in gene expression in $Tbr1^{layer6}$ mutants are due to direct regulation by TBR1, we performed chromatin immunoprecipitation sequencing (ChIP-seq) using P2 wild-type cortex. TBR1 binds to 68,218 regions genome-wide (Figure 3A). No enrichment was found at TBR1 ChIP-seq peaks in two different control datasets (input and negative [TBR1 blocking peptide and IgG]) (Figures 3A and S3A). Approximately 20% of peaks (13,973 peaks) overlap with transcription start site (TSS), 31% (21,189 peaks) are on gene body, 43% (29,010 peaks) are located intergenically, with 3% on exons (2,060 peaks), 2% on 3′ UTR (1,356 peaks), and 1% on 5′ UTR (630 peaks; Figure 3B). *De novo* motif discovery identified the canonical TBR1 binding motif in 17% of peaks (Figure 3B).

To gain further evidence that these peaks represent candidate regulatory elements (REs) influenced by TBR1, we assessed the number of genes with putative TBR1 regulatory loci that are dysregulated in the $Tbr1^{layer6}$ mutants (Figure 3D; Table S5). TBR1 binds to the 89% of the promoter regions and 77% of the candidate REs near the genes dysregulated in the $Tbr1^{layer6}$ mutants. Genes with TBR1 binding at the promoter, or with binding within 100 kb, exhibit higher overall expression levels relative to genes with no TBR1 binding (Figure S3B), indicating a general positive relationship between local TBR1 binding and gene expression. In contrast, there was no significant relationship between TBR1 promoter or distal binding and differential gene expression in the $Tbr1^{layer6}$ mutants (Figure S3C), likely due in part to the relatively high number of TBR1-binding sites. While we did not observe overall enrichment for TBR1 binding at DEX genes, regions that have both a TBR1 ChIP signal and a canonical TBR1 motif were enriched at promoters for genes downregulated in the $Tbr1^{layer6}$ mutants (Figure S3C).

We compared TBR1-bound regions to regions of open chromatin identified in fetal human cerebral cortex (germinal zone and cortical plate) (de la Torre-Ubieta et al., 2018), finding overlap between fetal human cortex assay for transposase-accessible chromatin using sequencing (ATAC-seq) with 80% of mouse TBR1-bound promoters and 23% of TBR1-bound distal regions. Compared to a control cardiac mesoderm ATAC-seq dataset (Koh et al., 2016), we found significant enrichment for TBR1 binding at open chromatin at both promoters and distal elements in fetal human cerebral cortex (Fisher's exact test, p value < 0.001), with no consistent differences in enrichment between ATAC-seq peaks specific to germinal zone or cortical plate (Figure S3D). Many DEX loci exhibited overlapping mouse TBR1 binding with human fetal cortex ATAC-seq regions (Figure S3E). This comparison demonstrates that the regulatory targets of TBR1 at P2 in the mouse cortex overlap with REs active in mid-fetal human cortical development.

We assessed the function of nine TBR1-bound REs containing a canonical TBR1 motif (T-box motif; Figures 3C and 3D; Table S6). RE expression vectors were transfected into P0 wild-type cortical cultures and assayed for luciferase activity 3 days later. In parallel, we co-transfected the RE vectors with a *Tbr1* expression vector. We tested 3 classes of putative REs that were candidates for regulating: (1) downregulated genes (*Tbr1*, *Foxp2*, *Grin2b*, and *Bcl11a*), (2) upregulated genes (*Hcn1*, *Fezf2*, and *Foxp1*), and (3) unchanged genes (*Dlx5/6*) (Tables S1 and S2). Luciferase activity was driven by all of the REs (Figure 3E), except the negative control *Dlx5/6, I56i* enhancer (active in forebrain GABAergic neurons) (Zerucha et al., 2000). *Tbr1* co-transfection only activated the *Tbr1*, *Foxp2*, *Grin2b*, and *Bcl11a* candidate REs, consistent with downregulation of these cognate genes in the $Tbr1^{layer6}$ mutants (Table S1; Figure 1A). Moreover, *Tbr1* co-transfection reduced luciferase expression with the *Hcn1*, *Fezf2* and *Foxp1* REs, which corresponded to the upregulated genes in the $Tbr1^{layer6}$ mutants (Table S1; Figure 1A).

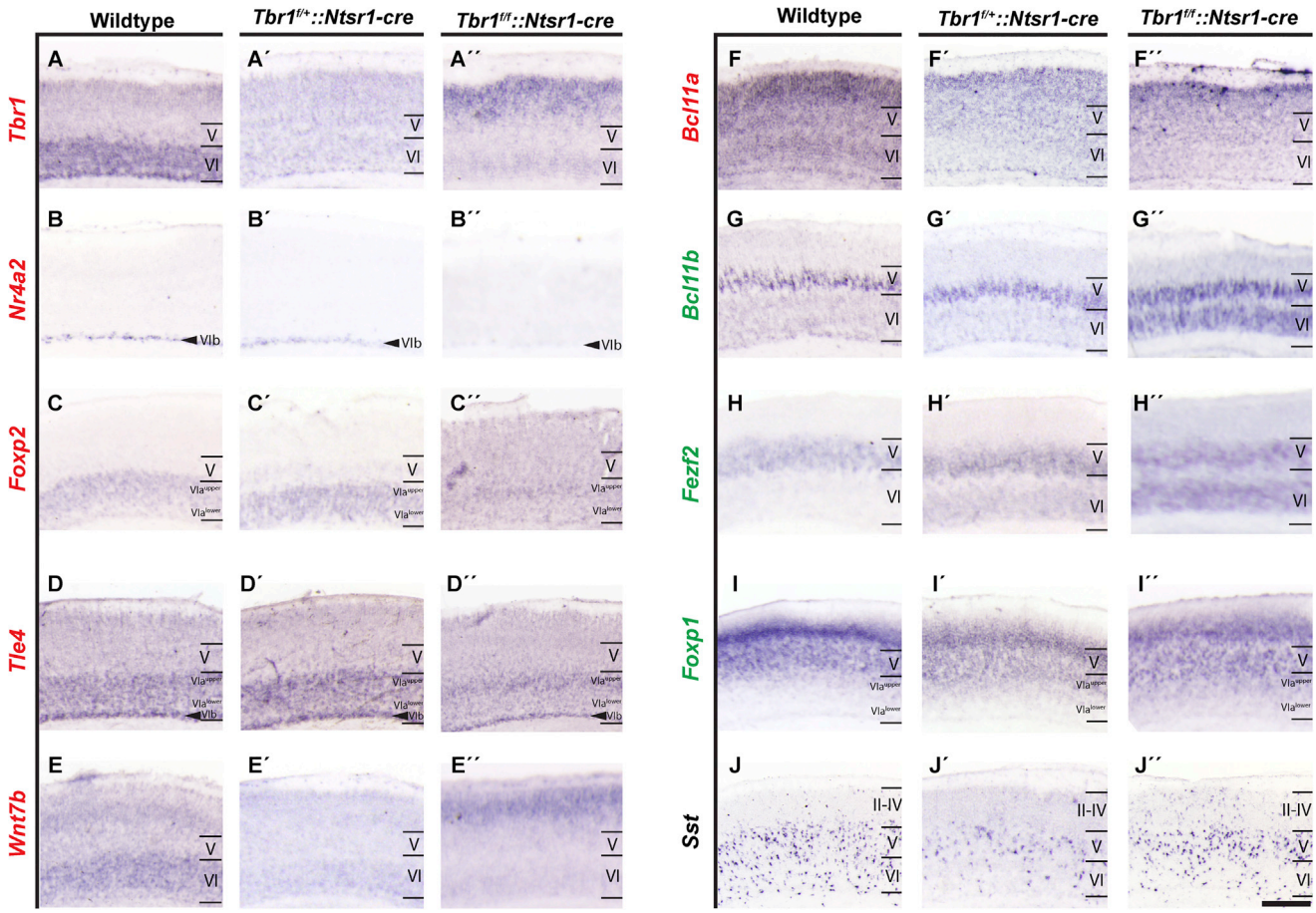

Figure 2. *Tbr1* Is Required to Maintain Layer 6 Identity in Postnatal Cortex

In situ hybridization on SSCx coronal sections of $Tbr1^{wild\text{-}type}$, (A′–J′) $Tbr1^{layer6}$ heterozygous (*Tbr1*$^{f/+}$*::Ntrs1-cre*), and (A″– J″) $Tbr1^{layer6}$ homozygous mutants *(Tbr1*$^{f/f}$*::Ntrs1-cre)* at P3 (n = 2). In $Tbr1^{layer6}$ heterozygotes and homozygotes, *Tbr1* (A–A″), *Nr4a2* (B–B″), *Wnt7b* (E–E″), and *Bcl11a* (F–F″) expression is reduced in layer 6 and the subplate. The expression of *Tbr1* and *Wnt7b* is increased in the superficial layers (A–A″ and E–E″). The expression of *Foxp2* (C and C″) and *Tle4* (D and D″) is reduced in layer $6a^{lower}$ of $Tbr1^{layer6}$ homozygous mutants. $Tbr1^{layer6}$ heterozygotes and homozygotes exhibit an ectopic expression of *Fezf2* (H–H″) in layer 6. In $Tbr1^{layer6}$ homozygous mutants, *Bcl11b* (G and G″) and *Foxp1* (I–I″) are ectopically expressed in layer 6. Furthermore, $Tbr1^{layer6}$ mutants exhibit changes in the number and laminar distribution of Sst^{+} CINs (J–J″). Transcriptome levels of each gene are reflected as downregulated (red), upregulated (green), or unchanged (black) in $Tbr1^{layer6}$ mutants. II–IV, layers 2–4; V, layer 5; VI, layer 6; VIb, subplate.
Scale bar, 50 μm. See also Figure S2 and Table S4.

Thus, using TBR1 ChIP-seq and an RE functional assay, we have identified REs that function either as activators or repressors in the presence of TBR1. These data solidify our evidence that TBR1 directly controls the molecular properties of layer 6 pyramidal neurons and that TBR1 functions as an activator or a repressor depending on the nature of the RE.

Tbr1 Specifies a Program that Patterns Apical Dendritic Lamination of Layer 6 Neurons

A key feature of a neuron's identity is its dendritic patterning (Lefebvre et al., 2015). Normally, the apical dendrites of layer 6 pyramidal neurons grow into layer 4 where they elaborate their branches (Ledergerber and Larkum, 2010). We used tdTomato expression driven by *Ntsr1-cre* in layer 6, to compare the dendritic patterning of wild-type and $Tbr1^{layer6}$ heterozygous and homozygous mutants (Figure 4). In the wild-type control, the apical dendrites of the layer 6 neurons extended to layer 4 at P3, P21, and P60 (Figures 4A–4C). On the contrary, the changes in the dendritic morphology of the $Tbr1^{layer6}$ heterozygotes were not detected at P3, began to emerge later in development at P21, and persisted into adulthood (P56) (Figure 4A′–4C′).

Interestingly, $Tbr1^{layer6}$ heterozygotes had two different subtypes of apical dendrites; first group extended to layer1 (white arrowheads) similar to those in the null (Figure 4A″–4C″), and a second group that extended to layers 2/3 (orange arrowheads) (Figure 4A′–4C′). On the other hand, in the $Tbr1^{layer6}$ homozygotes, the apical dendrites extended to layer 1 as early as P3, and these persisted into adulthood (P56) (Figure 4A″–4C″, white arrowheads). The change in dendritic morphology further supports the hypothesis that the mutant layer 6 neurons have layer-5-like properties. It is noteworthy that *Tbr1* also regulates dendritic patterning of retinal ganglion cells (Liu et al., 2018).

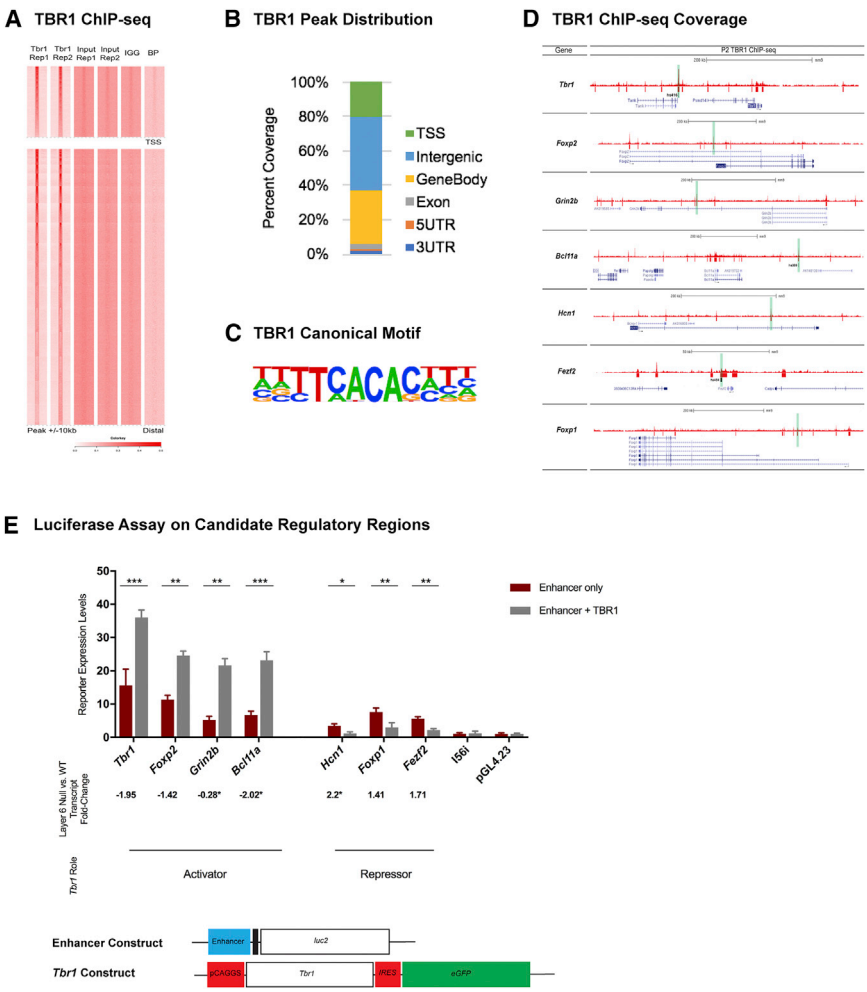

Figure 3. Genome-wide Analysis of TBR1 Binding and Transcriptional Regulation of Candidate Enhancer Regions in Loci Adjacent to *Tbr1*-Regulated Genes

(A) Heatmap of TBR1 ChIP-seq replicates compared to the controls.

(B) Summary of the genomic distribution of TBR1 ChIP-seq peaks at P2.

(C) TBR1 canonical motif.

(D) TBR1 ChIP-seq on wild-type whole cortex at P2 (red tracks). Red boxes represent the TBR1 binding that reached statistical significance. Genes are shown in blue. Candidate REs that were tested in the luciferase transcription assay are highlighted in green. Black boxes indicate REs that have proven enhancer activity in E11.5 cortex corresponding to hs416 (*Tbr1* locus), hs434 (*Fezf2* locus), and hs399 (*Bcl11a* locus). Black arrow indicates the direction of transcription. Genomic scale (in kilobases) is shown for each locus.

(E) Luciferase transcription assay was utilized to measure activity of *Tbr1*, *Foxp2*, *Grin2b*, *Bcl11a*, *Foxp1*, *Fezf2*, and *Hcn1* candidate enhancers in P0 primary cortical cultures. The reporter activity was measured under enhancer alone (red) and enhancer co-transfected with TBR1 (gray). TBR1 activates candidate REs of *Tbr1* (fold change [FC] = 2.3, p = 0.0007), *Foxp2* (FC = 2.17, p = 0.0023), *Grin2b* (FC = 4.11, p = 0.0015), and *Bcl11a* (FC = 3.46, p = 0.0002), whereas it represses candidate REs of *Foxp1* (FC = −2.52, p = 0.0087), *Fezf2* (FC = −2.55, p = 0.0015), and *Hcn1* (FC = −2.9, p = 0.0248). I56i enhancer and pGL4.23 empty vectors were used as negative controls.

The error bars represent SEM. Asterisk (*) represents the transcript fold-change using qPCR. t test with Welch's correction was used for the statistical analysis (*p < 0.05; **p < 0.01; ***p < 0.001). BP, blocking peptide; Rep1, replicate 1; Rep2, replicate 2; TSS, transcriptional start site.

See also Figure S4 and Tables S5 and S6.

Tbr1 Is Required after E17.5 for Corticothalamic Projections into the Anteromedial Thalamus

Layer 6 and subplate neurons extend their axons through the basal ganglia to the thalamus, where they form a stereotypic topographic map between cortical areas and specific thalamic nuclei (Deck et al., 2013). *Tbr1*^{constitutive} null axons fail to grow to the thalamus (Hevner et al., 2002). Here, we investigated corticothalamic projections in *Tbr1*^{layer6} mutants (Figure S4). Despite the evidence that *Tbr1*^{layer6} mutant neurons have molecular and dendritic properties of layer 5 neurons (Figures 1, 2, and 4), the mutant layer 6 neurons, like in the wild-type, have corticothalamic projections that enter the thalamus at P3 and P21 (Figures S4A and S4B). The quantification of the corticothalamic projections in *Tbr1*^{layer6} mutants demonstrates that this reduction was most strongly seen in the anterior and anteromedial thalamus of rostral coronal sections at P21 (regions 4 and 5; Figure S4C and S4D). However, *Tbr1*^{layer6} heterozygotes did not exhibit such deficit in their corticothalamic projections (data not shown).

To evaluate whether the phenotype was due to a failure to maintain the projections, or a failure to establish them, we studied neonatal *Tbr1*^{layer6} mutants at P3 (Figure S4A). The P3 and P21 phenotypes were very similar. Thus, while *Tbr1* is required prior to E17.5 for corticothalamic projections to emerge from the subpallium and enter the diencephalon (Hevner et al., 2001, 2002), these processes take place in the *Tbr1*^{layer6} mutants, consistent with the presence the functional TBR1 protein in the corticothalamic neurons when these cells are initially specified and grow their axons to the thalamus. However, the *Tbr1*^{layer6} mutants show that after ~E17.5, *Tbr1* is required for the maturation of corticothalamic connectivity preferentially in the anterior and anteromedial thalamus.

Excitatory Synapse Numbers Are Reduced in *Tbr1*^{layer6} Mutants at P21 and P56

We used immunofluorescence to label and analyze the excitatory presynaptic terminals (VGlut1^{+}) that are apposed to dendritic postsynaptic zones (PSD95^{+}) in the SSCx of *Tbr1*$^{wild\text{-}type}$ and *Tbr1*^{layer6} heterozygous and homozygous mutants on the apical spines of layers 6 neurons (n = 30) at P56 (Figure 5i) and P21 (Figure S5i). As depicted in Figure S5A, we examined the

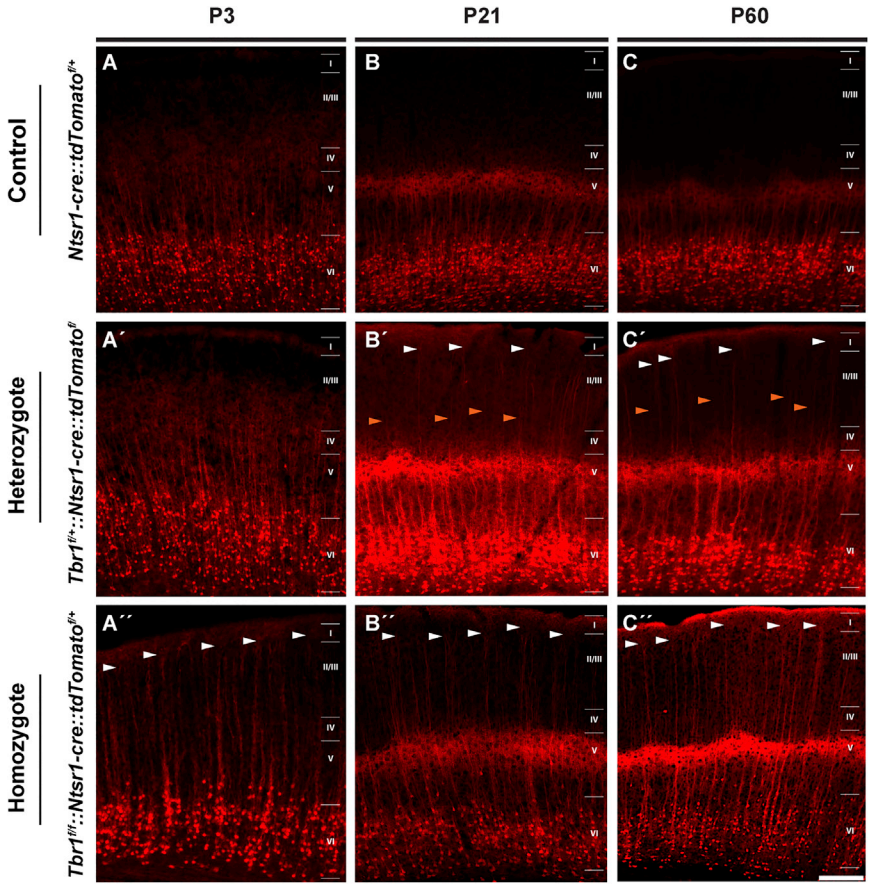

Figure 4. Ectopic Growth of Layer 6 Apical Dendrites into Superficial Layer 1 in *Tbr1*^{layer6} Mutants

The endogenous tdTomato fluorescence (red) in the SSCx of Control (*Ntsr1-cre::tdTomato*$^{f/+}$), (A′–C′) *Tbr1*^{layer6} heterozygous (*Tbr1*$^{f/+}$*::Ntsr1-cre::tdTomato*$^{f/+}$), and (A″–C″) *Tbr1*^{layer6} homozygous mutants (*Tbr1*$^{f/f}$*::Ntsr1-cre::tdTomato*$^{f/+}$). These mice had the *Ntsr1-cre::tdTomato*$^{f/+}$ alleles to label the layer 6 cell bodies and their dendrites. Changes in the dendritic patterning of layer 6 neurons were examined at P3 (A–A″), P21 (B–B″), and P56 (C–C″).

White arrowheads indicate some of the apical dendrites extending through layers 2/3 to layer 1 in *Tbr1*^{layer6} mutants. Orange arrowheads indicates a group of apical dendrites that only extend to layers 2/3. Cortical layers are labeled. Scale bar, 50 μm. See also Figure S4.

excitatory synapses in layer 5 of SSCx of *Tbr1*$^{wild\text{-}type}$ (*Ntsr1-cre::tdTomato*$^{f/+}$), *Tbr1*^{layer6} heterozygous (*Tbr1*$^{f/+}$*::Ntsr1-cre::tdTomato*$^{f/+}$), and *Tbr1*^{layer6} homozygous mutants (*Tbr1*$^{f/f}$*::Ntsr1-cre::tdTomato*$^{f/+}$; Figure S5A). Confocal fluorescent microscopy analysis of the synapse numbers showed a 30% decrease in *Tbr1*^{layer6} heterozygous (Bouton Density [BD] = 0.772, $p < 0.0001$) and 60% in *Tbr1*^{layer6} homozygous mutants at P56 (BD = 0.415, $p < 0.0001$; Figure 5A). The synaptic deficit phenotype was also present at P21, where excitatory synapse numbers were reduced by 34% in *Tbr1*^{layer6} heterozygous (BD = 0.501, $p < 0.0001$) and 64% in *Tbr1*^{layer6} homozygous mutants at P21 (BD = 0.273, $p < 0.0001$; Figure S5G).

To study the physiological ramification of reduced excitatory synaptic density in *Tbr1*^{layer6} mutants, we measured spontaneous excitatory postsynaptic currents (sEPSCs) using whole-cell patch clamp at P21 and P56. We recorded from neurons expressing *Ntsr1-cre*, identified using the fluorescent tdTomato Cre-dependent reporter, in SSCx from coronal slices of *Tbr1*$^{wild\text{-}type}$, *Tbr1*^{layer6} heterozygous, and *Tbr1*^{layer6} homozygous mutant (Figures S5A–S5C). The frequency of sEPSCs was reduced in *Tbr1*^{layer6} homozygous mutants as compared to cells from *Tbr1*$^{wild\text{-}type}$ mice at P56 (Figure 5B; n = 7/7/7, wild-type, heterozygous, homozygous [n = number of patched cells]; one-way ANOVA, $F_{(2,18)} = 10.17$, $p = 0.0011$; t test, Tukey correction, wild-type versus homozygous: $q_{(18)} = 6.371$, $p = 0.0008$). The decreased sEPSC frequency was also present at P21 (Figure S5I; n = 7/7/7, wild-type, heterozygous, homozygous; one-way ANOVA, $F_{(2,18)} = 6.625$, $p = 0.007$; t test, Tukey correction, wild-type versus homozygous: $q_{(18)} = 5.123$, $p = 0.0053$).

Tbr1^{layer6} Mutants Exhibit Altered Cortical Interneuron Lamination and Reduced Inhibitory Synaptic Density

The pattern of *Sst*$^{+}$ cortical interneurons (CINs) and their lamination is abnormal in the SSCx of P3 *Tbr1*^{layer6} mutants (Figure 2J–2J″). *Tbr1*^{layer6} heterozygotes exhibited a decrease in the *Sst*$^{+}$ CINs in layers 5 and 6 (Figures 2J, 2J′, and S3A), whereas in *Tbr1*^{layer6} homozygotes, the *Sst*$^{+}$ CINs were reduced in layer 6, unchanged in layer 5, and increased in layers 2–4 (Figures 2J, 2J″, and S3A). The reduction in *Sst*$^{+}$ CINs was persistent at P21 (data not shown). However, there were no changes in *PV*$^{+}$ CINs at P21 (Figure S3B).

We suggest that the *Tbr1*^{layer6} mutation disrupts the laminar distribution of *Sst*$^{+}$ CINs by altering the signals coming from the dendrites of the misspecified layer 6 pyramidal neurons. This result, in conjunction with the reduction in excitatory synapses, led us to measure inhibitory synapse numbers in the *Tbr1*^{layer6} mutants. From confocal images, we counted the numbers of inhibitory terminals (VGat^{+} presynaptic structures) apposed to dendritic postsynaptic zones (Gephyrin^{+}) onto the apical dendrites of layers 6 neurons (n = 30) of *Tbr1*$^{wild\text{-}type}$ and *Tbr1*^{layer6} heterozygous and homozygous mutants at P56 (Figure 5ii) and P21 (Figure S5ii). Analysis of inhibitory synapse numbers showed a 33% decrease in *Tbr1*^{layer6} heterozygous (BD = 0.673, $p < 0.0001$) and 66% in *Tbr1*^{layer6} homozygous mutants at P56 (BD = 0.346, $p < 0.0001$; Figure 5C). This phenotype was also detectable at P21, where the inhibitory synapse numbers were reduced 37% in *Tbr1*^{layer6} heterozygous mutants (BD = 0.574, $p < 0.0001$) and 72% decrease in *Tbr1*^{layer6} homozygous mutants (BD = 0.252, $p < 0.0001$) at P21 (Figure S5M).

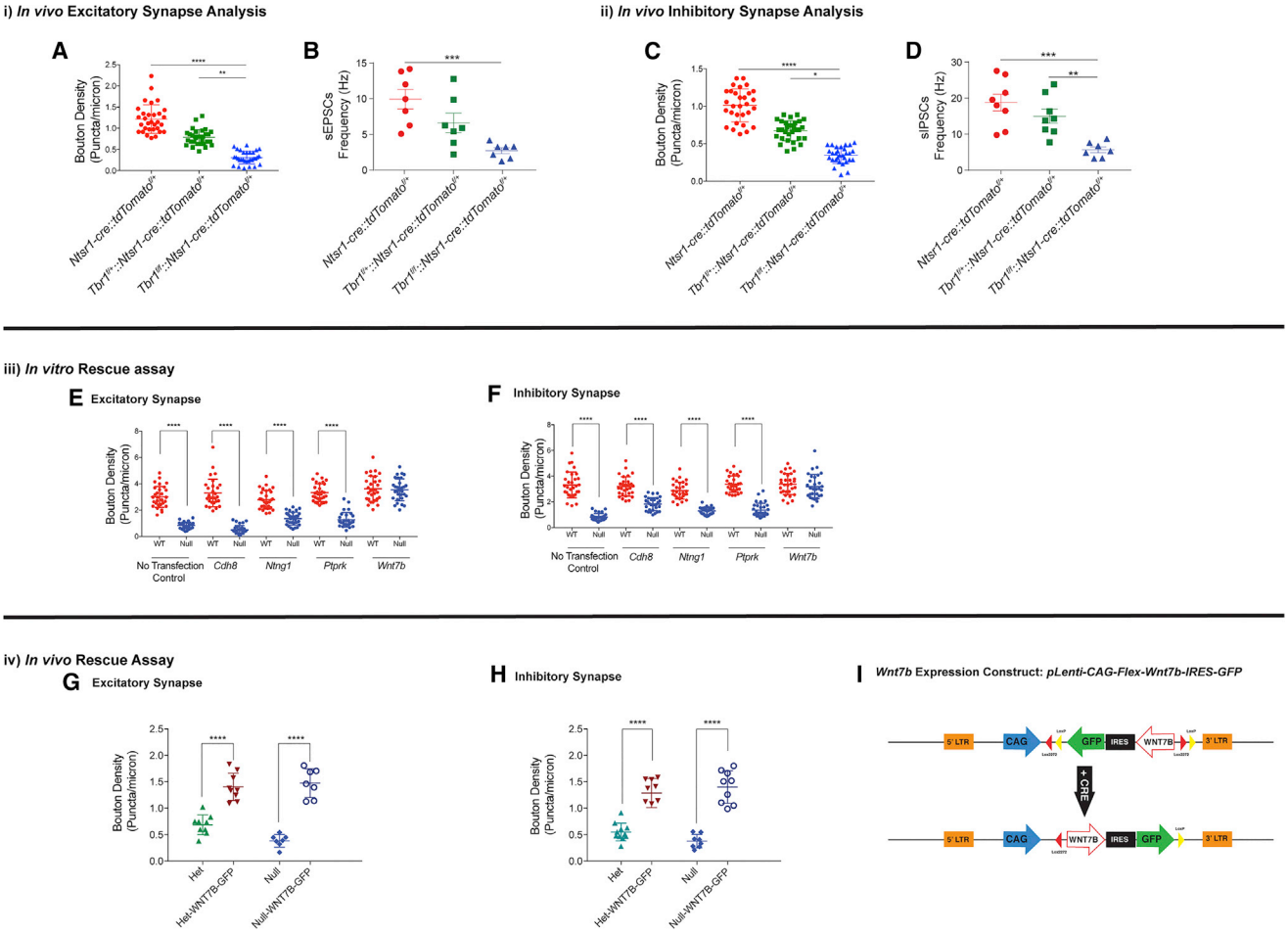

Figure 5. *Tbr1* Is Required for the Excitatory and Inhibitory Synaptic Development of Layer 6 Pyramidal Neurons at P56

(i) Excitatory synapses were analyzed via synaptic bouton staining onto apical dendrites of layer 6 neurons (n = 30) and spontaneous EPSC (sEPSC) recordings from the soma of *Tbr1* $^{\text{wild-type}}$ and *Tbr1*^{layer6} heterozygous and *Tbr1*^{layer6} homozygous mutants at P56. *Ntsr1-cre::tdTomato*$^{f/+}$ allele was used to label the layer 6 neurons. ImageJ software was used to process confocal images for quantification. Excitatory synapses were analyzed by VGlut1^{+} boutons and PSD95^{+} clusters co-localizing onto the dendrites of layer 6 neurons.

(A) Quantification of excitatory synaptic density at P56.

(B) Quantification of the sEPSC frequency in layer 6 neurons at P56.

(ii) Inhibitory synapses were examined by synaptic bouton staining onto apical dendrites of layer 6 neurons and spontaneous IPSC (sIPSC) recordings from the soma of the layer 6 neurons of *Tbr1* $^{\text{wild-type}}$ and *Tbr1*^{layer6} heterozygous and *Tbr1*^{layer6} homozygous mutants at P56. Inhibitory synaptic input was measured by VGat^{+} boutons and Gephyrin^{+} clusters co-localizing onto the dendrites of layer 6 neurons.

(C) Quantification of inhibitory synaptic density at P56.

(D) Quantification of the sIPSC frequency in layer 6 neurons at P56.

(iii) *In vitro* rescue assay was conducted using *Cdh8*, *Ntng1*, *Ptprk*, and *Wnt7b* expression vectors in cultured P0 cells from *Tbr1*$^{\text{wild-type}}$ (red) and *Tbr1*^{layer6} mutant (blue) (n = 2).

(E and F) Quantification of excitatory (E) and inhibitory (F) synaptic density *in vitro*.

(iv) *In vivo* rescue assay was conducted by injecting *Wnt7b-IRES-GFP* lentivirus into the layer 6 of SSCx of *Tbr1*^{layer6} heterozygous and *Tbr1*^{layer6} homozygous mutants at P1.

(G and H) Quantification of excitatory (G) and inhibitory (H) synapse numbers onto the layer 6 neurons of *Tbr1*^{layer6} heterozygous (Het) and *Tbr1*^{layer6} homozygous mutants (Null) expressing GFP at P21.

(I) Schematic representation of the lentiviral *CAG-Flex-Wnt7b-IRES-GFP* (*Wnt7b-IRES-GFP* expressing) construct. CRE inverts the *Wnt7b* coding region enabling its expression.

Error bars represent the SEM of all excitatory and inhibitory synapse numbers measured from each genotype. Two-way ANOVA was used for the statistical analysis of the control, heterozygote, and null. Two-tailed t test with Tukey correction was used for pairwise comparisons (*$p < 0.05$; **$p < 0.01$; ***$p < 0.001$; ****$p < 0.0001$). See also Figure S5.

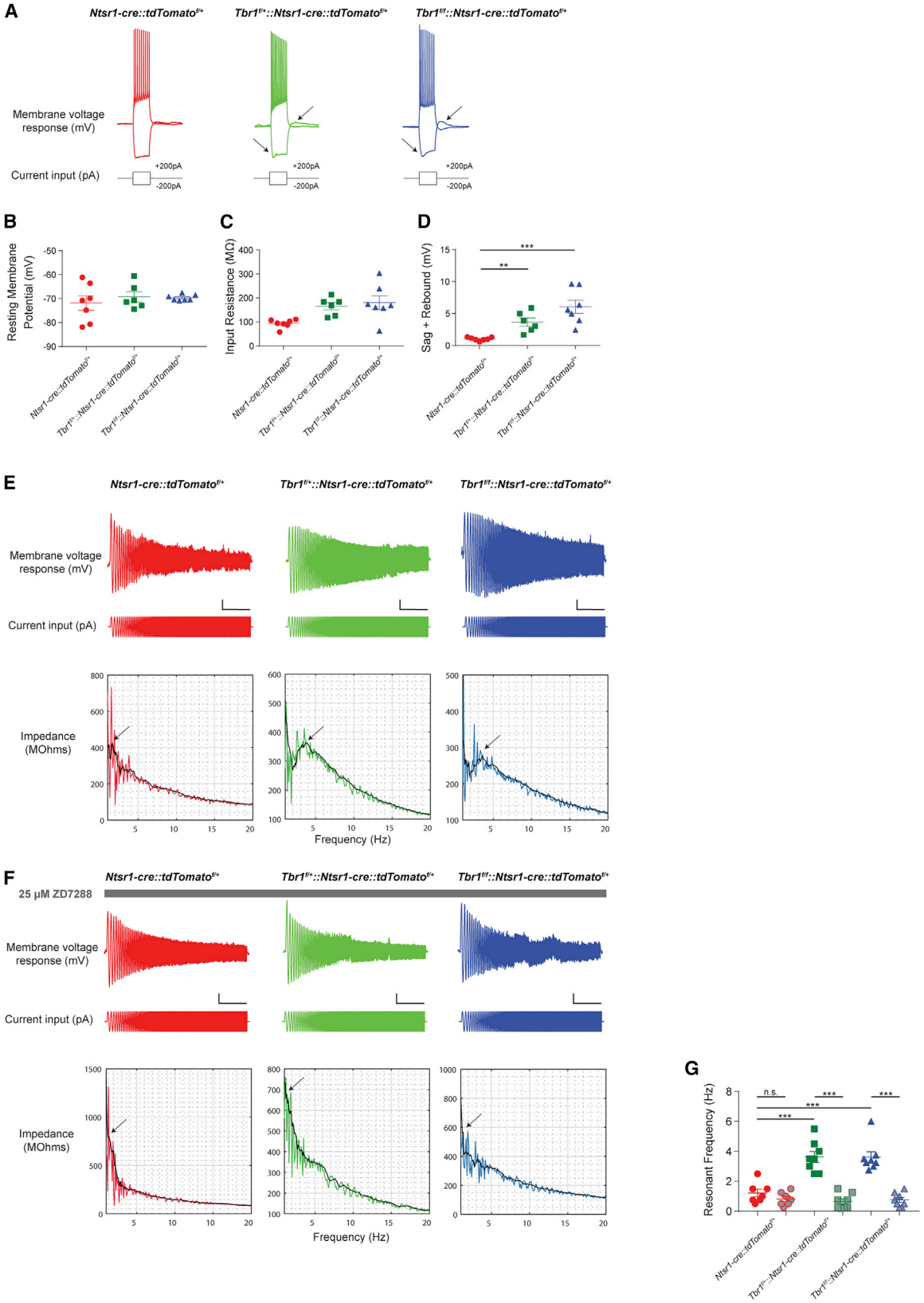

(legend on next page)

To test whether the reduced inhibitory synaptic density in *Tbr1*^{layer6} mutants had physiological ramifications, we measured spontaneous inhibitory postsynaptic current (sIPSCs) using whole-cell patch clamp on brain slices at P21 and P56. The frequency of sIPSCs were reduced in *Tbr1*^{layer6} homozygotes at P56 (Figure 5D; n = 8/8/7, wild-type, heterozygous, homozygous; one-way ANOVA, $F_{(2,20)} = 12.44$, $p = 0.0003$; t test, Tukey correction, wild-type versus homozygous: $q_{(20)} = 6.907$, $p = 0.0003$, heterozygous versus homozygous: $q_{(20)} = 4.901$, $p = 0.0066$). The reduction in sIPSC frequency was also present at P21 (Figure S5O; n = 7/6/7, wild-type, heterozygous, homozygous; one-way ANOVA, $F_{(2,17)} = 4.738$, $p = 0.023$; t test, Tukey correction, wild-type versus homozygous: $q_{(17)} = 3.847$, $p = 0.037$, heterozygous versus homozygous: $q_{(17)} = 3.635$, $p = 0.0495$). Lastly, we did not observe any changes in the amplitude of sEPSCs and sIPSCs at P21 and P56 (data not shown).

Restoring *Wnt7b* Expression Rescues the Decreased Synaptic Phenotype of *Tbr1*^{layer6} Mutant Neurons *In Vitro* and *In Vivo*

The decrease in the excitatory and inhibitory synaptic density in the layer 6 mutant neurons, in conjunction with the transcriptome changes in *Tbr1*^{layer6} FACS-purified neurons, prompted us to identify a subset of genes that are dysregulated in *Tbr1*^{layer6} mutant neurons that may contribute to the synaptic deficit. These genes, including *Cdh8* (Friedman et al., 2015; Liu et al., 2018), *Ntng1* (Zhang et al., 2016), *Ptprk* (Lim et al., 2009), and *Wnt7b* (Budnik and Salinas, 2011), have been shown to contribute to synaptic development, maintenance, and/or plasticity. Thus, we examined the impact of transfecting *Cdh8*, *Ntng1*, *Ptprk* and *Wnt7b* expression vectors in primary cortical cultures derived from *Tbr1*$^{wild\text{-}type}$ and *Tbr1*^{layer6} mutant neurons at P0 (n = 2).

After 14 days *in vitro*, we analyzed the number of excitatory (VGlut$^+$ presynaptic and PSD95$^+$ postsynaptic) and inhibitory (VGat$^+$ presynaptic and Gephyrin$^+$ postsynaptic) terminals of *Tbr1*$^{wild\text{-}type}$ and *Tbr1*^{layer6} homozygous mutant neurons (Figure 5iii). The reduced excitatory and inhibitory synaptic density was recapitulated *in vitro*, where excitatory and inhibitory synapse numbers were reduced by 71% (BD = 0.945, $p < 0.0001$) and 78% (BD = 0.836, $p < 0.0001$), respectively (Figures 5E and 5F).

Among the four tested genes, only *Wnt7b* rescued the reduction in both excitatory (Figure 5E) and inhibitory (Figure 5F) synapse numbers. Therefore, we further investigated the impact of *Wnt7b* expression on rescuing synapse numbers *in vivo* (Figure 5iv). We generated a flex lentiviral constructs that would express WNT7B and GFP upon *Cre* recombination (Figure 5I). We injected the *Wnt7b-IRES-GFP* lentivirus into layer 6 of SSCx of *Tbr1*^{layer6} heterozygotes and homozygotes at P1. The virus was only injected in the right hemisphere; the left hemisphere was used as a control. We analyzed excitatory and inhibitory synapse numbers on the apical dendrites of layer 6 neurons at P21 (Figures 5G and 5H). The regions expressing GFP in layer 6 cells showed an increase in excitatory and inhibitory synapse numbers (Figures 5G and 5H), thus providing *in vivo* evidence that restoring *Wnt7b* expression can rescue the synaptic deficits of *Tbr1*^{layer6} mutants.

Tbr1 Mutants Have Increased Hyperpolarization-Activated Cation Currents

We next examined the intrinsic properties of layer 6 neurons in *Tbr1*^{layer6} mutants using whole-cell patch clamp to measure intrinsic physiological properties of *Ntsr1-cre::tdTomato*$^+$ neurons of layer 6 in SSCx (Figure 6). Resting membrane potential (Figures 6B and S6B) and input resistance (Figures 6C and S6C) were not different between *Tbr1*$^{wild\text{-}type}$, *Tbr1*^{layer6} heterozygotes, and *Tbr1*^{layer6} homozygotes (n = 8) at P56 (Figure 6) and P21 (Figure S6).

A prominent feature of many layer 5 pyramidal neurons that is largely absent from layer 6 is a hyperpolarization-activated cation current (I_h or h-current) mediated by HCN channels (Shepherd, 2013). I_h causes a characteristic "sag" and "rebound" in current clamp recordings of responses to steps of hyperpolarizing current. We examined responses to a −200 pA step and found that SSCx layer 6 pyramidal neurons from P56 *Tbr1*^{layer6} heterozygotes and homozygotes exhibited significantly increased "sag + rebound" compared to *Tbr1*$^{wild\text{-}type}$ controls, suggesting increased I_h, while other intrinsic electrophysiological properties were largely unaltered (Figure 6D; n = 7/6/7, wild-type, heterozygous, homozygous; one-way ANOVA, $F_{(2,17)} = 13.18$, $p = 0.0003$; t test, Tukey correction, wild-type versus heterozygous: $q_{(17)} = 3.693$, $p = 0.0457$; wild-type versus homozygous: $q_{(17)} = 7.258$, $p = 0.0002$). Likewise, the neurons from *Tbr1*^{layer6} homozygotes at P21 also exhibited an increased I_h compared to *Tbr1*$^{wild\text{-}type}$ controls (Figure S6D; n = 8/8/8, wild-type, heterozygous, homozygous; one-way ANOVA, $F_{(2,21)} = 17.68$, $p < 0.001$; t test, Tukey correction, wild-type versus homozygous: $q_{(21)} = 8.331$, $p < 0.0001$; heterozygous versus homozygous: $q_{(21)} = 5.16$, $p = 0.0041$). Furthermore, HCN1 protein levels were increased ~5-fold in *Tbr1*^{layer6} homozygotes compared to *Tbr1*$^{wild\text{-}type}$ controls (Figures S6E and S6F), suggesting that upregulation of HCN1 could be contributing to the changes in the I_h of *Tbr1*^{layer6} mutant neurons.

Figure 6. Loss of *Tbr1* in Layer 6 Somatosensory Cortex Results in an Increase in Hyperpolarization-Activated Cation Currents

(A–C) Whole-cell patch clamp recordings from layer 6 SSCx at P56 (A) show that many intrinsic electrophysiological properties were unaffected by loss of *Tbr1*, including resting membrane potential (B), input resistance (C), and action potential half-width (data not shown).

(D) "Sag and rebound" is increased in *Tbr1*^{layer6} mutant neurons.

(E) Neurons were held in current clamp at −70 mV. The resonant frequency was measured as the frequency at which the impedance profile reached its peak (arrows). Scale bar, 5 mV, 5 s.

(F) ZD7288, an HCN channel blocker, decreased resonance frequency by over 50% in *Tbr1*^{layer6} heterozygous (green) and *Tbr1*^{layer6} homozygous mutants (blue).

(G) Quantification of changes in resonant frequency of *Tbr1*$^{wild\text{-}type}$ (red), *Tbr1*^{layer6} heterozygous (green) and *Tbr1*^{layer6} homozygous mutants (blue) after ZD7288 treatment.

Error bars represent the SEM of all recorded layer 6 neurons using whole-cell patch clamp from each genotype. $^{**}p < 0.01$; $^{***}p < 0.001$). See also Figure S6.

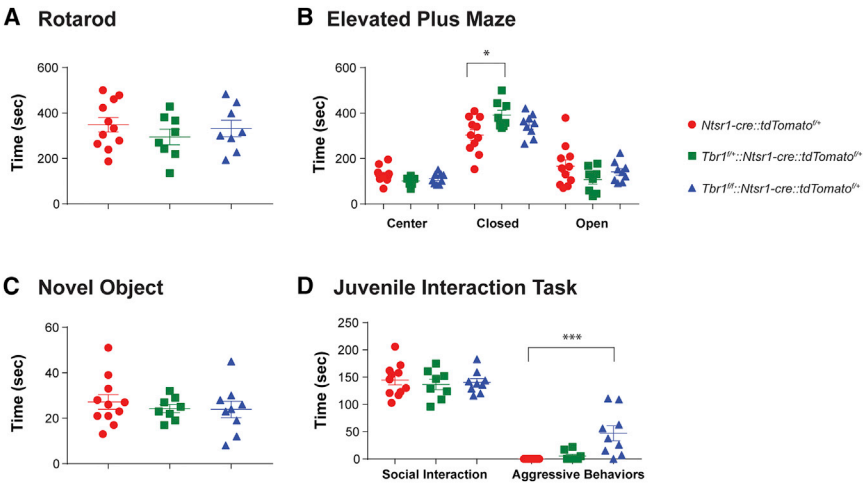

Figure 7. *Tbr1*^{layer6} Mutants Exhibit Increased Aggressive and Anxiety-like Behavior at P56–P80

Behavioral analysis of *Tbr1*$^{wild\text{-}type}$ (red), *Tbr1*^{layer6} heterozygous (green), and *Tbr1*^{layer6} homozygous mutants (blue).

(A) Rotarod assay did not demonstrate any impaired movement or motor coordination in *Tbr1*^{layer6} mutants.

(B) *Tbr1*^{layer6} heterozygous (green) mutants spent more time in the closed arm of the elevated plus maze (an anxiety-like phenotype) compared to their *Tbr1*$^{wild\text{-}type}$ littermates.

(C and D) Loss of *Tbr1* did not affect the time spent engaged in novel object exploration (C) or social interactions (D). *Tbr1*^{layer6} homozygous mutants (blue) exhibited aggressive behaviors when interacting with a novel juvenile mouse (D).

Error bars represent the SEM of all tested animals from each genotype. Two-tailed t test with tukey correction was used for pairwise comparisons (*$p < 0.05$; ***$p < 0.001$).

In deep-layer neocortical pyramidal neurons, the presence of I_h shifts the resonant frequency toward higher frequencies (Dembrow et al., 2010). Therefore, to further characterize potential increases in I_h in *Tbr1*^{layer6} mutants, we estimated the resonant frequency. For this, we injected constant current to hold *Ntsr1-cre*$^{+}$ neurons in current clamp near −70 mV and then introduced a sinusoidal current stimulus with constant amplitude (100 pA peak to peak) and a frequency that increased linearly from 0 to 20 Hz over 20 s (Figure 6E). We used the ratio of the fast Fourier transform of the voltage response (Figure 6E, top) to the fast Fourier transform of the sinusoidal current stimulus (Figure 6E, middle) to calculate the impedance amplitude profile (Figure 6E, bottom). We defined the resonant frequency as the frequency at which the impedance profile reached its peak. *Tbr1*^{layer6} heterozygous and *Tbr1*^{layer6} homozygous mutants exhibited an increase in their resonant frequency compared to *Tbr1*$^{wild\text{-}type}$ controls at P56 (Figure 6G; n = 7/8/8, wild-type, heterozygous, homozygous; one-way ANOVA, $F_{(2,20)} = 16.24$, $p < 0.0001$; t test, Tukey correction, wild-type versus heterozygous: $q_{(20)} = 7.075$, $p = 0.0002$; wild-type versus homozygous: $q_{(20)} = 7.038$, $p = 0.0002$).

Finally, we blocked I_h by bath applying the specific HCN channel antagonist ZD7288 (25 μM; Figure 6F). The resonant frequency was reduced by over 50% in the *Tbr1*^{layer6} heterozygous (Figure 6G; n = 8; paired t test, $t(7) = 7.723$, $p < 0.0001$) and *Tbr1*^{layer6} homozygous mutants (Figure 6G; n = 8; paired t test, $t(7) = 8.194$, $p < 0.0001$). However, the resonant frequency was not significantly altered by ZD7288 in neurons from *Tbr1*$^{wild\text{-}type}$ mice, indicating that I_h contributes to intrinsic resonance in mutant, but not wild-type, layer 6 pyramidal neurons. Thus, both *Tbr1*^{layer6} heterozygotes and homozygotes have an increased I_h resembling that of layer 5 neurons.

Tbr1 Mutants Exhibit Increased Aggressive and Anxiety-like Behaviors

To identify behavioral abnormalities linked to loss of *Tbr1* function in layer 6 neurons, we performed assays in littermate cohorts of *Tbr1*$^{wild\text{-}type}$, *Tbr1*^{layer6} heterozygous and homozygous mutant male and female mice between P56 and P80. *Tbr1*^{layer6} heterozygous and *Tbr1*^{layer6} homozygous mutants did not show impairments in locomotion as measured by speed in the open field (data not shown) or in motor coordination as measured by performance on a rotarod (Figure 7A) compared to wild-type controls. *Tbr1*^{layer6} mutants did not differ in the amount of time spent in the center of the open field (data not shown). However, in the elevated plus maze, *Tbr1*^{layer6} heterozygous mutants spent more time in the closed arms, suggesting an increase in anxiety-like behavior (Figure 7B; n = 11/8/9, wild-type, heterozygous, homozygous; one-way ANOVA, $F_{(2,25)} = 4.155$, $p = 0.028$; t test, Tukey correction, wild-type versus heterozygous: $q_{(25)} = 4.065$, $p = 0.022$).

To assay mouse social behavior, we measured the time each experimental animal spent exploring a novel object and a novel juvenile wild-type mouse of the same sex introduced to its home cage. There were no differences in the time *Tbr1*^{layer6} mutants spent exploring a novel object (Figure 7C). However, the *Tbr1*^{layer6} homozygous mutants spent more time with the novel juvenile mouse (Figure 7D; n = 11/8/9, wild-type, heterozygous, homozygous; one-way ANOVA, $F_{(2,25)} = 4.534$, $p = 0.021$; t test, Tukey correction, wild-type versus homozygous: $q_{(25)} = 3.731$, $p = 0.0364$). To further assess the type of interaction, we divided this time into "social interaction," defined as time spent in sniffing, close following, or allo-grooming, versus "aggressive" behavior, defined as biting, fighting, or close following associated with periods of active fighting. *Tbr1*$^{wild\text{-}type}$ and *Tbr1*^{layer6} heterozygous and homozygous mutants spent similar time in social interaction (Figure 7D). However, *Tbr1*^{layer6} homozygous mutants exhibited a marked increase in aggressive interactions with the juvenile (Figure 7D; n = 11/8/9, wild-type, heterozygous, homozygous; one-way ANOVA, $F_{(2,25)} = 10.97$, $p = 0.0004$; t test, Tukey correction, wild-type versus homozygous: $q_{(25)} = 6.237$, $p = 0.0005$). These data indicate that neonatal *Tbr1* deletion in layer 6 neurons in adult mice

leads to increased anxiety-like behavior in heterozygotes and increased aggressive behavior in homozygous mutants.

DISCUSSION

Neonatal *Tbr1* Specifies Properties of a Sublamina of Neocortical Layer 6 (Corticothalamic) and Represses Layer 5 (Corticofugal) Identity

Tbr1 is expressed in the excitatory neurons of the neocortex (subplate, layer 6, rostral layer 5, and layers 2/3), hippocampus, entorhinal cortex, pallial amygdala, piriform cortex, olfactory bulb, and CR neurons (Hevner et al., 2001, 2003). Analysis of $Tbr1^{constitutive}$ null mice demonstrated its function in the differentiation of the first waves of pallial glutamatergic neurons, including CR cells, olfactory bulb mitral cells, subplate cells, and layer 6 cells (Bedogni et al., 2010). Further analyses of $Tbr1^{constitutive}$ null mice revealed that *Tbr1* promotes the identity of layer 6 neurons by repressing layer 5 molecular properties in layer 6 (McKenna et al., 2011; Han et al., 2011).

Here, by deleting *Tbr1* late in gestation, we have demonstrated that *Tbr1* is required in maintaining subplate and layer 6 identity. The impaired differentiation of subplate and layer 6 neurons is indicated by molecular (Figures 1 and 2) and dendritic defects (Figure 4). $Tbr1^{layer6}$ mutant neurons have reduced expression of layer 6 markers, including *Wnt7b*, *Foxp2*, and *Tle4*, and have ectopic layer 6 expression of genes controlling layer 5 molecular properties, including *Bcl11b*, *Fezf2*, and *Foxp1*. Strikingly, the expression of *Tle4* and *Foxp2* are most strongly reduced in the deep part of layer 6 but is maintained in the subplate and the superficial part of layer 6. This result suggests the existence of layer 6 sublamina, which is consistent with a previous study (Chevée et al., 2018), that we refer to as layer $6a^{upper}$ and layer $6a^{lower}$. Subplate is considered layer 6b (Hoerder-Suabedsen et al., 2018). The ectopic expression of layer 5 markers in the $Tbr1^{layer6}$ mutants suggests that layer 6 mutant neurons have an altered fate that is a hybrid of layer 5 and layer 6 pyramidal neurons. This conclusion is supported by our computational transcriptomic analysis of DEX genes between layers 5 and 6 in wild-type at P5 and comparing those to the group of DEX genes from $Tbr1^{layer6}$ mutant neurons (Figure 1B). We discovered that 60% of the common genes between the two datasets changed in the same direction, demonstrating that $Tbr1^{layer6}$ mutant neurons share transcriptomic properties of layer 5 neurons. On the contrary, the remaining 40% of genes showed no significant change in the $Tbr1^{layer6}$ mutant neurons, showing that $Tbr1^{layer6}$ mutant neurons possess a hybrid fate of layer 5 and layer 6 neurons.

Despite their hybrid molecular characteristic, some phenotypes suggested a transformation toward layer 5 identity. For instance, dendritic patterning of layer 6 neurons resembled that of layer 5 neurons, as their apical dendrites extended superficially into the marginal zone (Lefebvre et al., 2015). In addition to changes in the transcriptome and in dendritic patterning, $Tbr1^{layer6}$ mutant neurons have increased I_h, similar to that of layer 5 neurons. There are at least two subclasses of pyramidal neurons within layer 5. Type B intratelencephalic (IT) cells lack prominent I_h, whereas type A corticofugal (CF) cells have a prominent I_h (Shepherd, 2013). In layer 6 of the $Tbr1^{layer6}$ mutants, the increase in I_h and levels of HCN1 protein suggests that the mutant layer 6 neurons have properties similar to type A layer 5 pyramidal neurons. Thus, *Tbr1* persistent function is required to initiate, orchestrate, and maintain a layer 6 specific program while repressing the layer 5 (specifically type A/CF) molecular, dendritic, and physiological program.

Contrary to $Tbr1^{constitutive\ null}$ mice, in which corticothalamic axons fail to grow into the thalamus (Hevner et al., 2001, 2002), $Tbr1^{layer6}$ mutants have corticothalamic projections that enter the thalamus. However, their intrathalamic ramifications are abnormal, with decreased projections in the anterior and anteromedial thalamus. Thus, even though *Tbr1* is required to initiate the corticothalamic pathway, it is not required to maintain these axons through P56 in the $Tbr1^{layer6}$ mutants. Furthermore, no ectopic subcortical projections or corpus callosum projections are generated by $Tbr1^{layer6}$ mutant neurons. Thus, despite taking on many layer 5 properties, the mutant layer 6 neurons do not grow layer-5-like axonal projections. Therefore, once the layer 6 axonal pathway choice program is established by *Tbr1*, it is irreversibly maintained in the absence of *Tbr1*. On the other hand, *Tbr1*-dependent programs for promoting layer 6 gene expression, repression of layer 5 gene expression, layer-6-specific dendritic patterning, and physiological properties (I_h) remain plastic and are dependent upon *Tbr1* function during the later stages of development and adulthood.

Overall, these results support our hypothesis that deleting *Tbr1* late in mouse gestation induces a hybrid fate in layer 6 and subplate neurons. $Tbr1^{layer6}$ mutant neurons transform to have many properties of layer 5 pyramidal neurons, including ectopic expression of regulators of layer 5 identity, dendritic patterning, and cell-intrinsic physiology, while also maintaining some aspects of layer 6 identity, such as their axonal projections to the thalamus.

Tbr1 Directly Regulates the Transcription of Genes that Control Layer 6 Identity

Toward elucidating TBR1-regulated transcriptional pathways that control layer 6 properties, we combined transcriptomic analysis of FACS-purified neonatal wild-type and $Tbr1^{layer6}$ mutant using whole-genome neonatal TBR1 ChIP-seq. These genomic analyses show that TBR1 directly regulates the transcriptional program driving layer 6 identity via genomic binding to gene promoters and distal enhancers. Our data further suggest that TBR1 interaction is mediated both by direct binding of TBR1 to the canonical or degenerate TBR1 motif and by secondary interaction, where the TBR1 motif is absent but TBR1 still interacts. Differential expression changes, especially for genes that control layer 6 identity, were more strongly associated with direct TBR1 binding to its cognate motif, as evidenced by ChIP-seq signal and putative motif presence at regulatory DNA elements associated with down- and upregulated genes. Despite these associations, TBR1 interaction, as identified via ChIP-seq alone, is not strongly indicative of an activating or repressive function. Furthermore, in general, TBR1 appears to be present at regulatory sequences of highly expressed genes in the P2 cortex. Investigation of the impact of *Tbr1* loss of function on chromatin state and transcriptional activation and repression, as has been done for other key transcriptional regulators (Sandberg et al., 2016), could further elucidate the regulatory function of TBR1 binding.

Transcription assays performed herein using neonatal primary cortical cultures demonstrated that TBR1 functions as an activator or repressor of specific REs adjacent to genes whose expression changes in *Tbr1*^{layer6} mutant neurons. Importantly, TBR1 activated REs near genes whose expression was reduced in layer 6 and repressed REs near genes whose expression was increased in layer 5. Future studies are needed to identify the nuclear co-factors that determine whether TBR1 acts as a transcriptional activator or repressor, although it is conceivable that the DNA sequence of the REs modifies TBR1's confirmation to control its activity. The discovery of these TBR1-regulated REs opens the possibility that these elements will show *in vivo* layer-specific activity that could be elucidated using transgenic experiments. These REs also serve as essential nodes for establishing the transcriptional circuits that drive TBR1-mediated gene expression, as well as sites where mutations may contribute risk for human neurodevelopmental disorders.

Tbr1 Is Required for Proper Synaptic Development in Layer 6 Neurons

A reduced density of excitatory and inhibitory dendritic synapses is a central phenotype of the *Tbr1*^{layer6} heterozygous and homozygous mutants, as seen in tissue sections from P21 and P56. A similar reduction was also seen in primary cultures grown from P0 cortex. These findings were substantiated using slice physiology, where *Tbr1*^{layer6} mutant neurons exhibit reduced sEPSCs and sIPSCs at P21 and P56. It is pertinent that *Tbr1*^{layer6} heterozygotes have reduced synapse numbers and reduced sEPSCs and sIPSCs, since *de novo Tbr1* loss-of-function mutations are found in the heterozygous state. Genes with synaptic function are enriched among ASD genes, suggesting this is a relevant pathway, although more work is needed to clarify this (Sanders et al., 2015). Therefore, the observed synaptic deficit in *Tbr1*^{layer6} mutants may be relevant to ASD. We further examined the impact of *Tbr1* loss of function on synaptogenesis and synaptic function by identifying a subset of *Tbr1*-regulated genes (66/178) that are linked to biological processes that could affect synapse development. These genes encode proteins implicated in signaling through G-protein-coupled receptors, WNTs, and retinoids, and that regulate cell adhesion (Table S1) (Yee and Chen, 2016).

WNT signaling is well known to control synapse development (Davis et al., 2008). WNTs promote synaptic assembly by signaling to the developing pre- and postsynaptic compartments (Budnik and Salinas, 2011; Salinas and Zou, 2008). Importantly, WNTs also are implicated in synaptic changes induced by neuronal activity in mature neurons (Budnik and Salinas, 2011). Here, we showed that restoring *Wnt7b* expression in *Tbr1*^{layer6} mutant neurons rescued the decrease in excitatory and inhibitory synapse numbers *in vitro* and *in vivo*. This provides evidence that downregulation of *Wnt7b* may contribute to the synaptic deficits in *Tbr1*^{layer6} mutants.

Currently, there are no effective somatic treatments for most core deficits of ASD. More broadly, there are no current treatments for neuropsychiatric illness in humans that restore normal biology. The ability to successfully restore synapse numbers by expressing *Wnt7b* may provide a possible avenue to restoring synapse numbers in humans with TBR1 mutations using small-molecule WNT7B agonists. In short, these observations provide an important initial step in conceptualizing rational therapies for ASD patients, although critically important hurdles remain, including demonstrating that the observed biology is truly relevant for pathology in humans and, if this is the case, determining at what developmental stages interventions may have an impact on core components of the ASD phenotype.

Tbr1^{layer6} Mutants Exhibit Increased Aggression and Anxiety-like Behaviors

Tbr1^{layer6} mutants are viable, allowing us to interrogate their behavior, which was remarkably normal in many assays, including assays of their motor functions (rotarod and open field) and interest in novel objects. On the other hand, *Tbr1*^{layer6} heterozygous mutants spent more time in the closed arms of the elevated plus maze, reflecting an increase in innate anxiety-like behaviors. Furthermore, homozygotes *Tbr1*^{layer6} mutants exhibited prolonged periods of aggression toward juvenile mice.

Ntsr1-Cre recombination of *Tbr1* does not extend into many cortical regions, including the olfactory bulb, dorsomedial neocortex (cingulate and retrosplenial), hippocampus and parahippocampus, piriform cortex, and pallial amygdala, ruling out the possibility that defects in *Tbr1*$^{+}$ neurons in these structures contribute to the behavioral phenotypes. This is pertinent, as *Tbr1*^{constitutive} heterozygotes have abnormal amygdala connectivity that has been associated with deficits in social interaction, cognitive flexibility, and associative memory (Huang et al., 2014). Thus, the highly specific molecular and physiological defects in the early-born pyramidal neurons of the neocortical subplate and layer 6 can be implicated in the mutants' increased aggression and anxiety-like behavior. While these phenotypes have similarities to common comorbidities of ASD, the relevance is unclear. However, it is relevant that loss of a single *Tbr1* copy in mouse leads to alterations in complex behaviors reflecting the type of circuit-based dysfunctions that likely underlie ASD.

Insights into How *Tbr1* Loss-of-Function Mutations Contribute Risk for ASDs

Genetic analyses of ASD patients have identified TBR1 as a high-confidence risk factor for ASD (Sanders et al., 2015). Analyses of co-expression networks of ASD risk genes provides evidence that reduced dosage of genes, such as *Tbr1*, may underlie ASD by disrupting processes in immature projection neurons of deep cortical layers during human mid-fetal development (Willsey et al., 2013). Here, by deleting *Tbr1* at a stage similar to the mid-fetal human, we have identified several novel *Tbr1* functions in mouse that provide hypotheses about how a reduction in *Tbr1* dosage may contribute to ASD pathophysiology.

As ASD loss-of-function mutations have their effect in the heterozygous state, a key discovery is that *Tbr1*^{layer6} heterozygous mice have a reduced density of excitatory and inhibitory dendritic synapses and reduced sEPSCs and sIPSCs. This supports a hypothesis that reduced TBR1 dosage increases ASD risk by reducing synaptic input onto layer 6 cortico-thalamic neurons. This model converges with the observation that many hcASD genes encode proteins that regulate synapse development and function (Sanders et al., 2015). *Tbr1*^{layer6} heterozygotes also had defects in dendritic patterning, an increased I_h, and

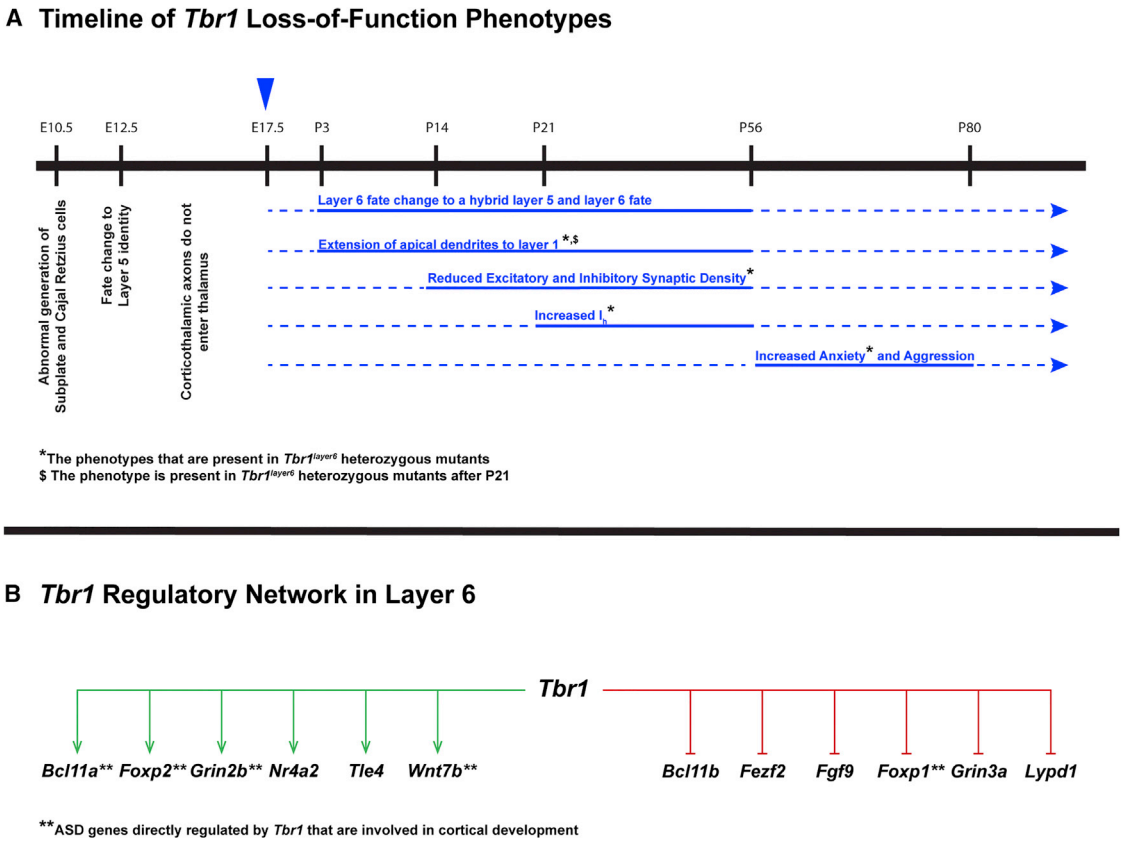

Figure 8. Summary of the Core Elements of a *Tbr1*-Driven Transcriptional Circuit in Neonatal Mouse Cortical Layer 6 Neurons

(A) Schematic representation of a timeline of *Tbr1* loss-of-function phenotypes from embryonic stages until adulthood in mouse. The blue arrowhead at E17.5 corresponds to the timing of knocking out *Tbr1* in layer 6 using conditional mutagenesis. Postnatal phenotypes associated with *Tbr1* loss of function are shown in blue. Solid lines correspond to the developmental window in which we have provided evidence for the reported phenotypes. Dotted lines represent the presumed duration of the reported phenotypes. Asterisk (*) indicates the phenotypes that are observed in $Tbr1^{layer6}$ heterozygotes and homozygotes.

(B) Schematic representation of regulatory network of *Tbr1* in cortical layer 6. *Tbr1* is a repressor (red) of determinants of layer 5 identity, including *Bcl11b, Fezf2*, *Fgf9*, *Foxp1*, *Grin3a*, and *Lypd1.* Conversely, *Tbr1* dictates layer 6 identity through activation (green) of layer 6 markers, including *Bcl11a*, *Foxp2*, *Grin2b*, *Nr4a2*, *Tle4*, and *Wnt7b.* Asterisks (**) indicate ASD genes directly regulated by *Tbr1* (TBR1 genomic binding and expression changes in the mutant) that are involved in cortical development.

anxiety-like behaviors in the elevated plus maze assay. While some of the other phenotypes detected in $Tbr1^{layer6}$ mutants were only present in the homozygotes, these observations could have relevance for ASD as they signify biological pathways that could be altered in *Tbr1* heterozygotes, including corticothalamic projections and aggression.

Furthermore, the transcriptome analysis revealed that *Tbr1* regulates other ASD genes, including *Scn2a1*, *Foxp1*, *Wnt7b*, *Nuak1* (Sanders et al., 2015), and *Foxp2* (Gong et al., 2004). *In situ* hybridization showed that *Bcl11a* expression, a probable ASD gene (Sanders et al., 2015), is also reduced in $Tbr1^{layer6}$ mutants. Additionally, previous work provided evidence that the $Tbr1^{constitutive\ null}$ regulates expression of ASD risk genes during cortical development (Notwell et al., 2016). Of the five reported TBR1 *de novo* mutations associated with ASD, two generate truncated proteins that lack the DNA-binding T-box domain. These TBR1 mutant proteins lose their ability to regulate transcription, have an altered intracellular distribution, and fail to interact with CASK (Huang and Hsueh, 2017) and FOXP2 (Deriziotis et al., 2014). Additional evidence of *Tbr1* involvement in molecular pathways relevant to ASD includes its regulation of *Grin2b*, *Bcl11a*, *Foxp1*, *Foxp2,* and *Wnt7b,* a subset of ASD genes that also regulate cortical development (Sanders et al., 2015). Furthermore, CASK phosphorylation of TBR1 by protein kinase A enhances TBR1's direct activation of *Grin2b* expression (Chuang et al., 2014).

In summary, we have elucidated core elements of a *Tbr1*-driven transcriptional circuit operating in neonatal mouse cortical layer 6 neurons (Figure 8). This program represses layer 5 transcriptomic properties, the layer 5 dendritic pattern, and layer-5-like I_h. It promotes and maintains cortical axons entering the thalamus and promotes excitatory and inhibitory synapse formation onto layer 6 pyramidal neurons. *Tbr1* is a hcASD gene and drives a transcriptional network that includes a subset of ASD genes, including *Scn2a1*, *Grin2b*, *Bcl11a*, *Foxp1*, *Nuak1*, and *Wnt7b*. Considering that $Tbr1^{layer6}$ heterozygotes, studied at a developmental stage that roughly approximates a point of convergent vulnerability in human pathology, have reduced

synapse numbers, sEPSCs, and sIPSCs and increased I_h, we propose that these phenotypes offer important new insights into how *Tbr1* loss-of-function mutations may contribute to ASD pathology in humans.

STAR★METHODS

Detailed methods are provided in the online version of this paper and include the following:

- KEY RESOURCES TABLE
- CONTACT FOR REAGENT AND RESOURCE SHARING
- EXPERIMENTAL MODEL AND SUBJECT DETAILS
  - Animals
  - Transgenic Animal Models
- METHOD DETAILS
  - Genomic DNA extraction and genotyping
  - RNA extraction and cDNA synthesis
  - Quantitative real time PCR (qPCR)
  - Western blot (WB)
  - RNA-Seq on FAC-Sorted Cells
  - Bioinformatics analysis of FAC-Sorted layer 6 RNA-Seq
  - TBR1 Chromatin immunoprecipitation (ChIP-Seq)
  - ChIP-Seq Computational Analysis
  - Primary Cell Culture and Luciferase assay
  - Lentiviral Injection and *in vivo* Rescue Assay
  - Histology
  - Image Acquisition and Analysis
  - Electrophysiology
  - Behavioral Assays
- QUANTIFICATION AND STATISTICAL ANALYSIS
- DATA AND SOFTWARE AVAILABILITY

SUPPLEMENTAL INFORMATION

Supplemental Information includes six figures and six tables and can be found with this article online at https://doi.org/10.1016/j.neuron.2018.09.027.

ACKNOWLEDGMENTS

This work was supported by research grants to J.L.R.R. (Nina Ireland, NIMH R37 MH049428, and NINDS R01 NS34661), V.S.S. (NIMH R01MH100292 and R01MH106507), and B.C. (NIH R01MH094589). A.S.N. and R.C.-P. were supported by NIGMS grant R35 GM119831, and R.C.-P. was supported via a Science Without Borders Fellowship from CNPq (Brazil).

AUTHOR CONTRIBUTIONS

Conceptualization, S.F.D., V.S.S., and J.L.R.R.; Methodology, S.F.D., S.E.R.S., Q.Q., J.D.M., R.C.-P., E.L.-L.P., A.R., S.K., D.T., A.S.N., A.J.W., B.C., V.S.S., and J.L.R.; Investigation, S.F.D., S.E.R.S., Q.Q., A.E., J.D.M., R.C.-P., S.K., D.T., and A.J.W.; Writing – Original Draft, S.F.D., S.E.R.S., B.C., A.J.W., V.S.S., and J.L.R.; Writing – Review & Editing, S.F.D., V.S.S., A.S.N., A.J.W., M.W.S., and J.L.R.R.; Funding Acquisition, A.S.N., A.J.W., B.C., M.W.S., V.S.S., and J.L.R.R.; Supervision, M.W.S. and J.L.R.R.

DECLARATION OF INTERESTS

J.L.R.R. is cofounder, stockholder, and currently on the scientific board of Neurona, a company studying the potential therapeutic use of interneuron transplantation. The remaining authors declare no competing interests.

Received: February 12, 2018
Revised: August 3, 2018
Accepted: September 14, 2018
Published: October 11, 2018

REFERENCES

Bedogni, F., Hodge, R.D., Elsen, G.E., Nelson, B.R., Daza, R.A.M., Beyer, R.P., Bammler, T.K., Rubenstein, J.L.R., and Hevner, R.F. (2010). *Tbr1* regulates regional and laminar identity of postmitotic neurons in developing neocortex. Proc. Natl. Acad. Sci. USA *107*, 13129–13134.

Budnik, V., and Salinas, P.C. (2011). Wnt signaling during synaptic development and plasticity. Curr. Opin. Neurobiol. *21*, 151–159.

Bulfone, A., Smiga, S.M., Shimamura, K., Peterson, A., Puelles, L., and Rubenstein, J.L.R. (1995). T-brain-1: a homolog of Brachyury whose expression defines molecularly distinct domains within the cerebral cortex. Neuron *15*, 63–78.

Bulfone, A., Wang, F., Hevner, R., Anderson, S., Cutforth, T., Chen, S., Meneses, J., Pedersen, R., Axel, R., and Rubenstein, J.L.R. (1998). An olfactory sensory map develops in the absence of normal projection neurons or GABAergic interneurons. Neuron *21*, 1273–1282.

Chevée, M., Robertson, J.J., Cannon, G.H., Brown, S.P., and Goff, L.A. (2018). Variation in activity state, axonal projection, and position define the transcriptional identity of individual neocortical projection neurons. Cell Rep. *22*, 441–455.

Chuang, H.-C., Huang, T.-N., and Hsueh, Y.-P. (2014). Neuronal excitation upregulates *Tbr1*, a high-confidence risk gene of autism, mediating *Grin2b* expression in the adult brain. Front. Cell. Neurosci. *8*, 280.

Chuang, H.-C., Huang, T.-N., and Hsueh, Y.-P. (2015). T-Brain-1: a potential master regulator in autism spectrum disorders. Autism Res. *8*, 412–426.

Cobos, I., Calcagnotto, M.E., Vilaythong, A.J., Thwin, M.T., Noebels, J.L., Baraban, S.C., and Rubenstein, J.L. (2005). Mice lacking *Dlx1* show subtype-specific loss of interneurons, reduced inhibition and epilepsy. Nat. Neurosci. *8*, 1059–1068.

Davis, E.K., Zou, Y., and Ghosh, A. (2008). Wnts acting through canonical and noncanonical signaling pathways exert opposite effects on hippocampal synapse formation. Neural Dev. *3*, 32.

de la Torre-Ubieta, L., Stein, J.L., Won, H., Opland, C.K., Liang, D., Lu, D., and Geschwind, D.H. (2018). The dynamic landscape of open chromatin during human cortical neurogenesis. Cell *172*, 289–304.e18.

De Rubeis, S., He, X., Goldberg, A.P., Poultney, C.S., Samocha, K., Cicek, A.E., Kou, Y., Liu, L., Fromer, M., Walker, S., et al.; DDD Study; Homozygosity Mapping Collaborative for Autism; UK10K Consortium (2014). Synaptic, transcriptional and chromatin genes disrupted in autism. Nature *515*, 209–215.

Deck, M., Lokmane, L., Chauvet, S., Mailhes, C., Keita, M., Niquille, M., Yoshida, M., Yoshida, Y., Lebrand, C., Mann, F., et al. (2013). Pathfinding of corticothalamic axons relies on a rendezvous with thalamic projections. Neuron *77*, 472–484.

Dembrow, N.C., Chitwood, R.A., and Johnston, D. (2010). Projection-specific neuromodulation of medial prefrontal cortex neurons. J. Neurosci. *30*, 16922–16937.

Deriziotis, P., O'Roak, B.J., Graham, S.A., Estruch, S.B., Dimitropoulou, D., Bernier, R.A., Gerdts, J., Shendure, J., Eichler, E.E., and Fisher, S.E. (2014). *De novo* TBR1 mutations in sporadic autism disrupt protein functions. Nat. Commun. *5*, 4954.

Friedman, L.G., Riemslagh, F.W., Sullivan, J.M., Mesias, R., Williams, F.M., Huntley, G.W., and Benson, D.L. (2015). Cadherin-8 expression, synaptic localization, and molecular control of neuronal form in prefrontal corticostriatal circuits. J. Comp. Neurol. *523*, 75–92.

Gong, X., Jia, M., Ruan, Y., Shuang, M., Liu, J., Wu, S., Guo, Y., Yang, J., Ling, Y., Yang, X., and Zhang, D. (2004). Association between the FOXP2 gene and autistic disorder in Chinese population. Am. J. Med. Genet. B. Neuropsychiatr. Genet. *127B*, 113–116.

Gong, S., Doughty, M., Harbaugh, C.R., Cummins, A., Hatten, M.E., Heintz, N., and Gerfen, C.R. (2007). Targeting Cre recombinase to specific neuron populations with bacterial artificial chromosome constructs. J. Neurosci. *27*, 9817–9823.

Han, W., Kwan, K.Y., Shim, S., Lam, M.M.S., Shin, Y., Xu, X., Zhu, Y., Li, M., and Šestan, N. (2011). TBR1 directly represses Fezf2 to control the laminar origin and development of the corticospinal tract. Proc. Natl. Acad. Sci. USA *108*, 3041–3046.

Hevner, R.F., Shi, L., Justice, N., Hsueh, Y., Sheng, M., Smiga, S., Bulfone, A., Goffinet, A.M., Campagnoni, A.T., and Rubenstein, J.L.R. (2001). Tbr1 regulates differentiation of the preplate and layer 6. Neuron *29*, 353–366.

Hevner, R.F., Miyashita-Lin, E., and Rubenstein, J.L.R. (2002). Cortical and thalamic axon pathfinding defects in Tbr1, Gbx2, and Pax6 mutant mice: evidence that cortical and thalamic axons interact and guide each other. J. Comp. Neurol. *447*, 8–17.

Hevner, R.F., Neogi, T., Englund, C., Daza, R.A.M., and Fink, A. (2003). Cajal-Retzius cells in the mouse: transcription factors, neurotransmitters, and birthdays suggest a pallial origin. Brain Res. Dev. Brain Res. *141*, 39–53.

Hoerder-Suabedsen, A., Hayashi, S., Upton, L., Nolan, Z., Casas-Torremocha, D., Grant, E., Viswanathan, S., Kanold, P.O., Clasca, F., Kim, Y., and Molnár, Z. (2018). Subset of cortical layer 6b neurons selectively innervates higher order thalamic nuclei in mice. Cereb. Cortex *28*, 1882–1897.

Huang, T.-N., and Hsueh, Y.-P. (2017). Calcium/calmodulin-dependent serine protein kinase (CASK), a protein implicated in mental retardation and autism-spectrum disorders, interacts with T-Brain-1 (TBR1) to control extinction of associative memory in male mice. J. Psychiatry Neurosci. *42*, 37–47.

Huang, T.-N., Chuang, H.-C., Chou, W.-H., Chen, C.-Y., Wang, H.-F., Chou, S.-J., and Hsueh, Y.-P. (2014). *Tbr1* haploinsufficiency impairs amygdalar axonal projections and results in cognitive abnormality. Nat. Neurosci. *17*, 240–247.

Koh, P.W., Sinha, R., Barkal, A.A., Morganti, R.M., Chen, A., Weissman, I.L., Ang, L.T., Kundaje, A., and Loh, K.M. (2016). An atlas of transcriptional, chromatin accessibility, and surface marker changes in human mesoderm development. Sci. Data *3*, 160109.

Ledergerber, D., and Larkum, M.E. (2010). Properties of layer 6 pyramidal neuron apical dendrites. J. Neurosci. *30*, 13031–13044.

Lefebvre, J.L., Sanes, J.R., and Kay, J.N. (2015). Development of dendritic form and function. Annu. Rev. Cell Dev. Biol. *31*, 741–777.

Lim, S.H., Kwon, S.K., Lee, M.K., Moon, J., Jeong, D.G., Park, E., Kim, S.J., Park, B.C., Lee, S.C., Ryu, S.E., et al. (2009). Synapse formation regulated by protein tyrosine phosphatase receptor T through interaction with cell adhesion molecules and Fyn. EMBO J. *28*, 3564–3578.

Liu, J., Reggiani, J.D.S., Laboulaye, M.A., Pandey, S., Chen, B., Rubenstein, J.L.R., Krishnaswamy, A., and Sanes, J.R. (2018). Tbr1 instructs laminar patterning of retinal ganglion cell dendrites. Nat. Neurosci. *21*, 659–670.

Long, J.E., Garel, S., Depew, M.J., Tobet, S., and Rubenstein, J.L. (2003). DLX5 regulates development of peripheral and central components of the olfactory system. J. Neurosci. *23*, 568–578.

Madisen, L., Zwingman, T.A., Sunkin, S.M., Oh, S.W., Zariwala, H.A., Gu, H., Ng, L.L., Palmiter, R.D., Hawrylycz, M.J., Jones, A.R., et al. (2010). A robust and high-throughput Cre reporting and characterization system for the whole mouse brain. Nat. Neurosci. *13*, 133–140.

McKenna, W.L., Betancourt, J., Larkin, K.A., Abrams, B., Guo, C., Rubenstein, J.L.R., and Chen, B. (2011). *Tbr1* and *Fezf2* regulate alternate corticofugal neuronal identities during neocortical development. J. Neurosci. *31*, 549–564.

Notwell, J.H., Heavner, W.E., Darbandi, S.F., Katzman, S., McKenna, W.L., Ortiz-Londono, C.F., Tastad, D., Eckler, M.J., Rubenstein, J.L.R., McConnell, S.K., et al. (2016). TBR1 regulates autism risk genes in the developing neocortex. Genome Res. *26*, 1013–1022.

Salinas, P.C., and Zou, Y. (2008). Wnt signaling in neural circuit assembly. Annu. Rev. Neurosci. *31*, 339–358.

Sandberg, M., Flandin, P., Silberberg, S., Su-Feher, L., Price, J.D., Hu, J.S., Kim, C., Visel, A., Nord, A.S., and Rubenstein, J.L.R. (2016). Transcriptional networks controlled by NKX2-1 in the development of forebrain GABAergic neurons. Neuron *91*, 1260–1275.

Sanders, S.J., He, X., Willsey, A.J., Ercan-Sencicek, A.G., Samocha, K.E., Cicek, A.E., Murtha, M.T., Bal, V.H., Bishop, S.L., Dong, S., et al.; Autism Sequencing Consortium (2015). Insights into autism spectrum disorder genomic architecture and biology from 71 risk loci. Neuron *87*, 1215–1233.

Shepherd, G.M.G. (2013). Corticostriatal connectivity and its role in disease. Nat. Rev. Neurosci. *14*, 278–291.

Vogt, D., Wu, P.-R., Sorrells, S.F., Arnold, C., Alvarez-Buylla, A., and Rubenstein, J.L.R. (2015). Viral-mediated labeling and transplantation of medial ganglionic eminence (MGE) cells for in vivo studies. J. Vis. Exp. *98*, 52740.

Willsey, A.J., Sanders, S.J., Li, M., Dong, S., Tebbenkamp, A.T., Muhle, R.A., Reilly, S.K., Lin, L., Fertuzinhos, S., Miller, J.A., et al. (2013). Coexpression networks implicate human midfetal deep cortical projection neurons in the pathogenesis of autism. Cell *155*, 997–1007.

Yee, A.X., and Chen, L. (2016). Differential regulation of spontaneous and evoked inhibitory synaptic transmission in somatosensory cortex by retinoic acid. Synapse *70*, 445–452.

Zerucha, T., Stühmer, T., Hatch, G., Park, B.K., Long, Q., Yu, G., Gambarotta, A., Schultz, J.R., Rubenstein, J.L., and Ekker, M. (2000). A highly conserved enhancer in the Dlx5/Dlx6 intergenic region is the site of cross-regulatory interactions between Dlx genes in the embryonic forebrain. J. Neurosci. *20*, 709–721.

Zhang, Q., Goto, H., Akiyoshi-Nishimura, S., Prosselkov, P., Sano, C., Matsukawa, H., Yaguchi, K., Nakashiba, T., and Itohara, S. (2016). Diversification of behavior and postsynaptic properties by netrin-G presynaptic adhesion family proteins. Mol. Brain *9*, 6.

STAR★METHODS

KEY RESOURCES TABLE

REAGENT or RESOURCE	SOURCE	IDENTIFIER
Antibodies		
Mouse anti-HCN1 monoclonal antibody	Millipore	Cat# MABN20; RRID: AB_10806489
Normal rabbit IgG antibody	SCBT	Cat# sc2027; RRID: AB_737197
Rabbit anti-Parvalbumin polyclonal antibody	Swant	Cat#PV28; RRID: AB_2315235
Rabbit anti-Cyclophilin B polyclonal antibody	Abcam	Cat# ab16045; RRID: AB_443295
Rabbit anti-TBR1 ploYclonal antibody	SCBT	Cat# sc-48816 X; RRID: AB_2287060
Goat anti-Rabbit HRP antibody	Thermo Fisher Scientific	Cat# 31460; RRID: AB_228341
Rabbit anti-Vglut1 polyclonal antibody	Synaptic Systems	Cat# 135303; RRID: AB_887875
Mouse anti-PSD95 antibody	NeuroMab (UC Davis)	Cat# 75-028; RRID: AB_2307331
Rabbit anti-Vgat polyclonal antibody	Synaptic Systems	Cat# 131002; RRID: AB_887871
Mouse anti-Gephyrin polyclonal antibody	Synaptic Systems	Cat# 147011; RRID: AB_887717
Goat anti-Rabbit IgG Alexa Fluor 488	Thermo Fisher Scientific	Cat# A-11008; RRID: AB_143165
Goat anti-Mouse Alexa Fluor 647	Thermo Fisher Scientific	Cat# A32728; RRID: AB_2633277
Bacterial and Virus Strains		
pLenti-CAG-Wnt7b-IRES-GFP	This paper	N/A
Chemicals, Peptides, and Recombinant Proteins		
Mouse anti-TBR1 Blocking peptide	Abcam	Cat# ab25853
Sucrose	Sigma Aldrich	S5016
Sodium bicarbonate ($NaHCO_3$)	Sigma Aldrich	S6014
Glucose	Sigma Aldrich	G5767
Magnesium sulfate ($MgSO_4$)	Sigma Aldrich	230391
Sodium phosphate monobasic monohydrate (NaH_2PO_4)	Sigma Aldrich	P9638
Potassium chloride (KCl)	Sigma Aldrich	P9333
Calcium chloride dehydrate ($CaCl_2$)	Sigma Aldrich	223506
Magnesium chloride dexahydrate ($MgCl_2$)	Sigma Aldrich	M9272
Potassium gluconate (KGluconate)	Sigma Aldrich	P1847
HEPES	Sigma Aldrich	H3375
EGTA	Sigma Aldrich	E4378
Adenosine 5′-triphosphate magnesium salt (Mg-ATP)	Sigma Aldrich	A9187
Guanosine 5′-triphosphate sodium salt hydrate (Na_3GTP)	Sigma Aldrich	51120
Cesium Methanesulfonate	Sigma Aldrich	C1426
Sodium Chloride (NaCl)	Sigma Aldrich	S9888
QX314 chloride	Tocris	2313
ZD7288	Tocris	1000
Critical Commercial Assays		
Ovation Ultralow System V2 (ChIP-seq)	NuGEN	Cat# 0344
TruSeq Stranded Total RNA Library Prep Gold	Illumina	Cat# 20020598
Bioanalyzer High Sensitivity DNA Kit	Agilent	Cat# 5067-4626
Bioanalyzer RNA 6000 Nano Kit	Agilent	Cat# 5067-1511

(*Continued on next page*)

Continued

REAGENT or RESOURCE	SOURCE	IDENTIFIER
Deposited Data		
TBR1 P2 ChIP-seq Raw and Analyzed Data	This paper	GEO: GSE119362
Experimental Models: Organisms/Strains		
Mouse TBR1 conditional mutant	This paper	N/A
Mouse TBR1 constitutive mutant	This paper	N/A
Oligonucleotides		
Primer for genotyping flox allele	This Paper	N/A
ND.for GAC ACA CAC CCT TCT TCA GTT TAC AGC		
ND.rev CAA GCC CGA CTG CCA ATG TTC TG		
Primer for genotyping Ntsr1-cre allele	This Paper	N/A
Ntsr1-cre.for GAC GCC ACG CCC CCC TTA		
Ntsr1-cre.rev CGG CAA ACG GAC AGA AGC ATT		
Primer for genotyping tdTomato allele	This Paper	N/A
tdTomato.for CTG TTC CTG TAC GGC ATG G		
tdTomato.rev GGC ATT AAA GCA GCG TAT CC		
Recombinant DNA		
For complete list of recombinant DNA, please refer to Table S4.	This Paper	N/A
Software and Algorithms		
ImageJ	N/A	https://imagej.nih.gov/ij/
MiniAnalysis	http://www.synaptosoft.com/MiniAnalysis/	v6.0.7
GraphPad Prism	https://www.graphpad.com/scientific-software/prism/	v7.01
MATLAB	https://www.mathworks.com/products/matlab.html	v8.6.0.267246
Clampex and Multiclamp	https://www.moleculardevices.com/products/axon-patch-clamp-system/acquisition-and-analysis-software/pclamp-software-suite	v10.2
ANY-maze	https://www.stoeltingco.com/any-maze-video-tracking-software-1224.html	v5

CONTACT FOR REAGENT AND RESOURCE SHARING

Further information and requests for resources and reagents should be directed to and will be fulfilled by the Lead Contact, Dr. John L. Rubenstein (john.rubenstein@ucsf.edu).

EXPERIMENTAL MODEL AND SUBJECT DETAILS

Animals

All procedures and animal care were approved and performed in accordance with the University of California San Francisco Laboratory Animal Research Center (LARC) guidelines. All strains were maintained on a C57BL/6 background. Animals were housed in a vivarium with a 12hr light, 12hr dark cycle. Postnatally, experimental animals were kept with their littermates. For timed pregnancies, noon on the day of the vaginal plug was counted as embryonic day 0.5.

The *Tbr1*^{flox} allele was generated by inGenious Targeting Laboratory (Ronkonkoma, NY). LoxP sites were inserted into introns 1 and 3, flanking *Tbr1* exons 2 and 3 (Figure 1A). To enable selection of homologous recombinants, the LoxP site in intron 3 was embedded in a *neo* cassette that was flanked by *Flp* sites. The *neo* cassette was removed by mating to a *Flp*-expressing mouse to generate the *Tbr1*^{flox} allele. Cre excision removes exons 2 and 3, including the T-box DNA binding region, similar to the constitutive null allele (Bulfone et al., 1998). *Ntsr1-cre* mice (Gensat 220) were used to delete *Tbr1* in layer 6 projection neurons. *tdTomato*$^{fl/+}$ (*Ai14*) mice were crossed with *Tbr1*$^{f/f}$ mice and used as an endogenous reporter. *Tbr1* layer 6 knockout mice (*Tbr1*^{layer6} mutant) were generated by crossing *Tbr1*$^{f/f}$*::tdTomato*$^{f/+}$ mice with *Tbr1*$^{f/+}$*::Ntsr1-cre*$^{+}$. The specific gender and age of experimental animals can be found in the Results section and corresponding figure legends.

Transgenic Animal Models

Information about the generation and genotyping of the transgenic lines used in this study can be found in the corresponding original studies: *Ntsr1-Cre* (Gong et al., 2007), lox-STOP-lox-tdTomato (Ai14; Madisen et al., 2010). Mice were maintained on C57BL/6J background.

METHOD DETAILS

Genomic DNA extraction and genotyping

Tissue samples were digested in a solution containing 1 mg/mL of proteinase K, 50 mM Tris-HCl pH 8.0, 100 mM EDTA, 100 mM NaCl and 1% SDS. Genomic DNA was extracted using a standard ethanol precipitation protocol. Genotyping was performed with PCR-based assays using purified genomic DNA, and primer-pair combinations flanking the deleted region and detecting *Cre* and *tdTomato* alleles.

RNA extraction and cDNA synthesis

Total RNA was extracted from the cortices of wild-type and *Tbr1* constitutive null mice at E15.5 and P0 using RNeasy Plus Mini Kit (QIAGEN) following the manufacturer's protocol. First strand cDNA was synthesized using Superscript reverse transcriptase II following manufacturer's protocol (Thermo Fisher).

Quantitative real time PCR (qPCR)

Quantitative RT-PCR was performed to measure RNA levels using SYBR Green (Bio-Rad) and 7900HT Fast Real-Time PCR System. Gene-specific primers for *Tbr1* exons 1, 2 and 4, *Bcl11a*, *Grin2b* and *Hcn1* as well as *ef1α* housekeeping genes (HKG) were designed using the Primer 3 program. The expression levels of the genes in both wild-type and *Tbr1* mutant mice were normalized to the expression levels of *ef1α*. Subsequently, the gene expression levels in *Tbr1* mutant mice were measured relative to the wild-type littermates.

Western blot (WB)

Cortices of 2 *Tbr1* constitutive null and 2 wild-type brains were dissected at E15.5 and P0 in ice-cold PBS. For assessing HCN1 protein levels, the SSCx was dissected in ice-cold HBSS from P7 mice. Cortices were dissociated using a Papain Dissociation System (Worthington Biochemical Corporation) following manufacturer's protocol. tdTomato^{+} cells were sorted using BD FACS Aria II Cell Sorter at Center for Advanced Technology (UCSF).

Tissues were homogenized in 300 μL ice-cold RIPA lysis buffer. Following an incubation at 4°C for 2 hr with agitation, the samples were centrifuged at 13,500 rpm for 20 min at 4°C. 20-30 μg total protein was combined with Laemmli buffer supplemented with 1:20 β-mercaptoethanol and was heat to 95°C for 5 min. The protein lysate was electrophoresed using Mini-PROTEINTGX 4%–20% precasted gels (Bio-Rad) and ran for 1-2 hr at 100V. The franctionated proteins were transferred to a nitrocellulose membrane (GE Amersham Protran). The membrane was blocked with 7.5% nonfat dried milk, washed 3X with 1X PBS with 0.1% Tween-20, and then was incubated for 12 hr with the primary antibody at 4°C. The following day, the membrane was washed 3X with 1X PBS with 0.1% Tween-20, incubated with the Goat Anti-Rabbit-HRP secondary for 1 hr. Signals were detected using a DAB system (Vector Laboratories) following manufacturer's protocol.

RNA-Seq on FAC-Sorted Cells

Layer specific transcriptome profiling was conducted by using RNA-seq on FAC-Sorted cells from SSCx of *Tbr1*$^{wild\text{-}type}$ *and Tbr1*^{layer6} mutants. The SSCx was dissected in HBSS from P5 mice (Thermo Fisher). Cortices were dissociated using a Papain Dissociation System (Worthington Biochemical Corporation) following manufacturer's protocol. tdTomato^{+} cells were sorted using BD FACS Aria II Cell Sorter at Center for Advanced Technology (UCSF). Approximately 25,000 cells were collected from each sample and immediately proceeded with RNA extraction using RNeasy Plus Micro Kit (QIAGEN) following manufacturer's protocol. using Agilent RNA 6000 Nano Kit (Agilent Technologies) and ran on Bioanalyzer 2100 (Agilent Technologies) and samples that had RIN scores of 8.5-9.5 were used to generate libraries. Library preparation and amplification was performed by TruSeq Stranded Total RNA Library Prep Kit with Ribo-Zero Gold Set A (Illumina). The amplification of adaptor-ligated fragments was carried out for 12 cycles during which individual index sequences were added to each distinct sample. Library concentration was assessed with Qubit (INFO) and library fragment size distribution was assessed on the Agilent Bioanalyzer 2100 (Agilent Technologies) and Agilent High Sensitivity DNA Kit (Agilent Technologies) following manufacturer's protocol. Libraries were validated using qPCR. Pooled, indexed RNA-seq libraries were sequenced on Hiseq 4000 at Center for Advanced Technology (UCSF) to produce 100 bp paired-end reads.

Bioinformatics analysis of FAC-Sorted layer 6 RNA-Seq

Collectively, we analyzed 8 RNA-Seq libraries, which comprised of 4 *Tbr1*$^{wild\text{-}type}$ layer 6, 5 *Tbr1*$^{wild\text{-}type}$ layer 5, and 4 *Tbr1*^{layer6} layer 6 mutant RNA-Seq libraries. Sequencing was conducted on HiSeq 4000 using Paired-End 100 (PE100) with the Library fragment size of approximately 300 bp.

RNA-Seq alignment, and quality control

The RNA-Seq reads were aligned to the mm9 mouse genome reference using STAR in gene annotation mode. Picard was utilized to generate alignment quality control (QC) metrics for every RNA-Seq samples. Principal component analysis (PCA) of the quality control matrices was employed to determine the presence of RNA-Seq sample outliers (The outliner is defined as a sample whose QC metrics are at least three standard deviations away from the mean in any of the first three principal components). The analysis did not indicate any outliers in layer 6 samples. We found and removed one outlier in layer 5 WT control samples. After quality control, we had 4 $Tbr1^{wild\text{-}type}$ layer 5, 4 $Tbr1^{wild\text{-}type}$ layer 6, and 4 $Tbr1^{layer6}$ layer 6 mutant samples.

Gene expression estimation and normalization

Gene expression was quantified with HTSeq in intersection-strict mode. We created two subsets of samples after obtaining raw gene expression counts. The first subset contained 4 layer 6 $Tbr1^{wild\text{-}type}$ and 4 layer 6 $Tbr1^{layer6}$ mutant samples. The second subset had 4 layer 5 $Tbr1^{wild\text{-}type}$ and 4 layer 6 $Tbr1^{wild\text{-}type}$ samples. We employed the same gene filtering and normalization approach to process both subsets of samples. We removed genes have less than or equal to one read in more than 50% of the samples. Filtered genes were normalized for gene length, GC content, and sample library size using CQN R-package. Gene length is obtained directly from the gene annotation file (.GTF) of mouse mm9 genome build reference. BedTools is used to compute the gene GC content. After normalization, the genes whose expression value don't change across all samples are removed. PCA is applied to identify any sample outliners with those filtered and normalized gene expression. The expression values were scaled and centered before PCA. PCA over gene expression shows that there are not outliers in the datasets.

Differential gene expression analysis (DEX analysis) with layer 6 $Tbr1^{wild\text{-}type}$ and $Tbr1^{layer6}$ mutant samples

To identify DEX genes, we identified all possible confounding variables including ribosomal bases in the mapped reads, percentage of bases in intronic region, RIN, Sex and RNA concentration to produce a reliable conclusion. Thousands of negative binomial regression models are built to model expressions of each genes. The best model is formed using Bayesian information criterion (BIC) and forward stepwise algorithm. The DEX analysis was performed with edgeR. Genes that pass a 0.05 significant threshold are considered as significantly DEX genes.

Differential gene expression analysis (DEX analysis) with layer 5 $Tbr1^{wild\text{-}type}$ and layer 6 $Tbr1^{wild\text{-}type}$ samples

Mice were of varying sex (4 males, 1 females in layer 5 wild-type versus 2 males and 2 females in layer 6 wild-type) and therefore we controlled for sex in DEX analyses. The DEX analysis was performed with edgeR. Significantly DEX genes are genes that pass a 0.05 significant threshold and have a $\log_2$fold change large than or equal to 1.5 or less than or equal to 1.5 ($\log_2$fold change $\geq$ 1.5 or $\log_2$fold change ≤ -1.5).

Comparison between DEX genes identified in two DEX analyses

We utilized three different analyses to examine the relationship between DEX gene lists identified by two comparisons. We used hypergeometric test to see what is the likelihood of observing an enrichment of "*layer 5* $Tbr1^{wildtype}$ versus layer 6 $Tbr1^{wildtype}$ DEX genes" in the "$Tbr1^{layer6}$ mutant versus layer 6 $Tbr1^{wildtype}$ DEX gene list." We conducted permutation test to further study this relationship without having the hypergeometric distribution assumption. The permutation test was run for 500,000 times to ensure we obtained a highly accurate underline distribution. P value of the permutation test was defined as proportion of randomly generated gene lists that have at least the same number of overlapped gene as what we observed in our dataset. We determined the background for these calculations as the number of overlapped genes in two DEX analyses. In additional to the enrichment tests, we studied gene expression pattern of our data. Genes with same effect direction are genes that are 1) up in "layer 6 $Tbr1^{layer6}$ mutant versus layer 6 $Tbr1^{wildtype}$" and "*layer 5* $Tbr1^{wildtype}$ versus layer 6 $Tbr1^{wildtype}$". 2) down in "layer 6 $Tbr1^{layer6}$ mutant versus $Tbr1^{wildtype}$" and "*layer 5* $Tbr1^{wildtype}$ versus layer 6 $Tbr1^{wildtype}$." Genes with opposite effect direction are genes that are 1) up in "layer 6 $Tbr1^{layer6}$ mutant versus layer 6 $Tbr1^{wildtype}$" and down in "*layer 5* $Tbr1^{wildtype}$ versus layer 6 $Tbr1^{wildtype}$" or 2) down in "layer 6 $Tbr1^{layer6}$ mutant versus layer 6 $Tbr1^{wildtype}$" and up in "*layer 5* $Tbr1^{wildtype}$ versus layer 6 $Tbr1^{wildtype}$."

Layer specific gene set enrichment analysis

We conducted hypergeometric test to examine the relationship between the significant DEX genes identified in "layer 6 $Tbr1^{wildtype}$ versus $Tbr1^{layer6}$ mutant" comparison and layer specific genes reported by Willsey et al. (2013). Willsey et al. provided a list of layer specific genes in Table S5. The mouse samples used in our experiments are estimated to be most similar to P4 and P5 developing cells. Therefore, we restricted our analysis to genes layer specific at P4 and P5. We used a hypergeometric test (one-sided) to assess enrichment. We determined the background for these calculations as the number of filtered genes in our dataset.

TBR1 Chromatin immunoprecipitation (ChIP-Seq)

Transcription factor ChIP was performed as previously published with a few modifications (McKenna et al., 2011; Sandberg et al., 2016). P2 somatosensory cortices were dissected and dissociated by pipetting in cold PBS. Dissociated cells were fixed in 1% formaldehyde for 10 min at RT and neutralized with 1 mL 2.5M glycine. Fixed chromatin was lysed and sheared into 200 - 1,000 bp fragments using a Covaris S2 (14 cycles of duty cycle = 5%, intensity = 3 and cycles per burst = 200). Immunoprecipitation (IP) reactions of two biological replicates at P2 were performed using 5 μg TBR1 polyclonal antibody (Santa Cruz Biotech, SC48816 X (M-200)). 20X molar excess TBR1 blocking peptide was used as negative control. Protein/antibody complexes were collected using Dynabeads (20 mL protein A + 20 mL protein G). ChIP-seq libraries were generated using Ovation Ultralow System V2 (NuGEN) following manufacturer's protocol. The resulting libraries were size selected (180–350 bp) and sequenced at the Center for Advanced Technology at UCSF (Illumina HiSeq 4000; http://cat.ucsf.edu/) using a single read 50-bp strategy.

ChIP-Seq Computational Analysis

Clustering, base calling, and quality metrics were performed using standard Illumina software. Sequenced libraries were analyzed for overall quality and were filtered to remove artifacts and low-quality sequences using Trim Galore version 0.4.2 (https://www.bioinformatics.babraham.ac.uk/projects/trim_galore/), and reads were mapped to the mouse genome (mm9) using BWA version 0.7.16a: bwa aln -t 12 mm9 sample.trimmed.fastq.gz).

Significant binding peaks were called on individual replicates using MACS version 2.1.0 against matched input control and blocking peptide negative control samples, with both the model-based peak identification and local significance testing disabled: *macs2callpeak -t chip.bam -c input.bam -n chip_vs.input -f BAM -g mm–call-summits -B -q 0.01–nolambda–nomodel–extsize = 350–outdir output_directory*

Downstream analyses were conducted on merged peaks across replicates, filtered to remove ENCODE blacklisted regions and annotated using custom scripts. Coverage plots and heatmap diagrams were generated using ngs.plot version 2.61. We performed *de novo* motif discovery and enrichment analysis of significant known motifs using HOMER version 4.9 with default settings and genomic background. Plots of motif distribution around peaks and heatmaps were generated using custom R scripts (data not shown). The data used in this publication have been deposited in NCBI's Gene Expression Omnibus (GEO) under accession number GEO: GSE119362 (https://www.ncbi.nlm.nih.gov/geo/query/acc.cgi?acc=GSE119362); ChIP-seq experiments can be visualized in the UCSC genome browser via track hubs that are hosted at https://github.com/NordNeurogenomicsLab/Publications/tree/master/Darbandi_Cell_2018.

TBR1 ChIP-seq peaks from P2 mouse cortex defined here were compared to regions of open chromatin identified via ATAC-seq analysis of micro-dissected human fetal cerebral cortex (germinal zone and cortical plate; de la Torre-Ubieta et al., 2018) and to a human embryonic stem cell derived cardiac mesoderm dataset (Koh et al., 2016) as an unrelated tissue. Called peaks from the human ATAC-seq datasets were annotated to the mouse genome via the UCSC liftover tool and overlap was compared between the human fetal cortex and control peaks for promoter and distal regions. The proportion of TBR1-bound peaks from each ATAC-seq dataset was compared via Fisher's exact test.

Primary Cell Culture and Luciferase assay

Plasmids

To generate luciferase constructs candidate REs of mouse *Tbr1* (hs416, chr2: 61494203-61494886, 683bp), *Foxp2* (chr6: 15097241-15098146, 905 bp), *Grin2b* (chr6: 135813640-135814770, 1,130 bp), *Bcl11a* (chr11: 24270818-24271924, 1,383 bp), *Hcn1* (chr13: 118669041-118670541, 1,500 bp), *Fezf2* (hs434, chr14: 13170235-13171693, 1,458bp), *Foxp1* (chr6: 99325484-99327361, 1,877 bp), and *Dlxl5/6i* enhancer (chr6: 6819420-6819819, 400 bp) were amplified by PCR, and cloned into the pGL4.23 vector (Promega). The vectors were transformed with *DH5α E. coli* cells at 42°C.

Luciferase assay

Primary cortical neurons were harvested from P0 wild-type cortex and transfected using Lipofectamine 2000 (Invitrogen) and one of the RE luciferase vectors that were generated as described above. To test whether TBR1 modified the REs activity, *pCAG-Tbr1-IRES-eGFP* was co-transfected together with one of the aforementioned RE vectors. A renilla luciferase plasmid (pRL, Promega) was co-transfected to control for transfection efficiency. The luciferase assay was performed 48hrs after transfection using the dual-luciferase kit (Promega) according to manufacturer's instructions. Reporter activity was measured using Veritas Microplate Luminometer (Turner BioSystems, Model# 9100-001).

Primary Cell Culture

Cortex was dissected from P0 $Tbr1^{wild\text{-}type}$ and $Tbr1^{layer6}$ homozygous mutants and dissociated using papain dissociation kit following manufacturer's protocol (Worthington). A total of 100,000 cells were seeded into tissue culture slides pre-coated with poly-L-lysine (10 mg/ml, Sigma) and then laminin (5 mg/ml, Sigma), and grown *in vitro* with media containing DMEM-H21 with 5% fetal bovine serum for 2 hr. After the cells recovered, DMEM-H21 media was replaced by Neurobasal medium containing B27 supplement, 25% glucose, and glutamax overnight. $Tbr1^{layer6}$ mutant cells were transfected with *Cdh8*, *Ntng1*, *Ptprk* and *Wnt7b* expression vectors and $Tbr1^{wild\text{-}type}$ were transfected with mock empty vector using Lipofectamine 2000 (Invitrogen) for 6 hr. Following incubation, the media was replaced by Neurobasal medium containing B27 supplement, Penicillin/Streptomycin, 25% glucose, and glutamax. Cultures were grown for 14 days *in vitro*. Cultures were fixed with 4% PFA for 10 min and processed for immunohistochemistry. Briefly, they were washed in PBS, quenched 2 times for 15 min with 2 mg/ml sodium borohydrate solution, blocked in PBS containing 10% Normal Serum, 0.1% Triton X- 100 and 2% BSA, incubated in primary antibody overnight (4°C), washed in PBS, incubated in secondary antibody for 1-2 hr (room temperature), washed in PBS, and mounted. This experiment was repeated twice (n = 2).

Lentiviral Injection and *in vivo* Rescue Assay

In vivo rescue assay was carried out by cloning *Wnt7b* into a *Cre*-dependent lentiviral backbone (*pLenti-CAG-Flex-Wnt7b-IRES-GFP*). HEK293T cells were transfected with *pLenti-CAG-Flex-Wnt7b-IRES-GFP* and *pLenti-BG-GFP-T2a-Cre* using Polyplus jetPRIME transfection reagent following manufacturer's protocol. WNT7B levels were examined by performing western blot against WNT7B on HEK293T cell lysates that were transfected previously. Upon validation, the *Wnt7b-IRES-GFP* expressing lentivirus

(*pLenti-CAG-Flex-Wnt7b-IRES-GFP*) was generated in HEK293T cells as previously reported (Vogt et al., 2015) using Polyplus jetPRIME transfection reagent following manufacturer's protocol.

Lentivirus expressing *Wnt7b-IRES-GFP* was injected in the SSCx of *Tbr1*^{layer6} heterozygous and homozygous mutants pups at P1. For injections, a glass micropipette of 50 μm diameter (with a beveled tip) was preloaded with sterile mineral oil and viral suspension was front-loaded into the tip of the needle using a plunger connected to a hydraulic drive (Narishige) that was mounted to a stereotaxic frame. P1 pups from *Tbr1*^{layer6} wild-type and *Tbr1*^{layer6} heterozygous and homozygous mutants were anesthetized on ice for 1–2 min before injections. Each pup received 3–5 viral injections (70 nL per site) in the right hemisphere. These sites were about 1 mm apart along the rostral to caudal axis. Viral suspensions were injected into layer 6 of the neonatal SSCx. After injections, pups were put back with the mother to recover after they began to move around on their own. Mice were sacrificed 21 days after injection and transcardially perfused with PBS followed by 4% PFA.

Histology

At the time of experiment, for P0 and P3 experiments, animals were anesthetized on ice while postnatal (P21 and P56) animals were anesthetized with intraperitoneal avertin (0.015 ml/g of a 2.5% solution) injection. Animals were perfused transcardially with cold PBS and then with 4% PFA in PBS, followed by brain isolation, 1-2 hr post-fixation, cryoprotected in 30% sucrose in PBS, and cut frozen (coronally or sagittally) on a sliding microtome at 40μm for immunohistochemistry or *in situ* hybridization. All primary and secondary antibodies were diluted in PBS containing 10% Normal Serum, 0.25% Triton X-100 and 2% BSA. The following primary antibodies were used: Chicken anti-GFP (1:2000, Aves), mouse anti-Vglut1 (1:200, Synaptic Systems), rabbit anti-Vgat (1:500, Synaptic Systems), rabbit anti-PSD95 (1:200, Cell Signaling), mouse anti-gephyrin (1:200, Synaptic Systems). The secondary antibodies for immunofluorescence were Alexa Fluor-conjugated and purchased from Thermofisher. For synapse immunohistochemistry, a total of n = 30 apical dendrites were counted from each of *Tbr1*$^{wild\text{-}type}$, *Tbr1*^{layer6} heterozygous and *Tbr1*^{layer6} homozygous mutants. The coronal sections were pre-treated with pepsin to enhance the staining. Immunofluorescence specimens were counterstained with 1% DAPI to assist the delineation of cortical layers. For *in situ* hybridization a rostro-caudal coronal series of at least ten sections from n = 2 brains from *Tbr1*$^{wild\text{-}type}$ and *Tbr1*^{layer6} homozygous mutants were examined. Anti-sense riboprobes for *Tbr1*, *Nr4a2*, *Foxp2*, *Tle4*, *Wnt7b*, *Cntn2*, *Ptprk, Bcl11a, Bcl11b*, *Fezf2*, *Foxp1* and *Sst* were prepared as previously described (Cobos et al., 2005; Long et al., 2003). ISH was performed using digoxigenin-labeled riboprobes.

Image Acquisition and Analysis

Fluorescent and bright-field images were taken using a Coolsnap camera (Photometrics) mounted on a Nikon Eclipse 80i microscope using NIS Elements acquisition software (Nikon). Confocal imaging experiments were conducted at the Cancer Research Laboratory (CRL) Molecular Imaging Center, supported by Helen Wills Neuroscience Institute at UC Berkeley. Confocal images were acquired using Zeiss LSM 880 with Airyscan with a 63X objective at 1,024 × 1,024 pixels resolution using ZEN 2.0 software. Brightness and contrast were adjusted, and images merged using Photoshop or ImageJ software. ImageJ software was used for image processing. For synapse counting (presynaptic and postsynaptic boutons), confocal image stacks (0.4μm step size) were processed with ImageJ software. In brief, background subtraction and smooth filter were applied to each stack. Using a threshold function, each stack was converted into a 'masks' image. Furthermore, the channels were co-localized with the Image Calculator plugging. Lastly, the number of co-localizations were counted, and the length of each dendrite was measured in each of the focal plane. Staining for control and mutant were done in parallel as well as the image capturing.

Electrophysiology

Coronal brain slices (250 μm) including SSCx were made from three mice (n = 3) at age p21-28 and at p56-p80. Slicing solution was chilled to 4°C and contained (in mM): 234 sucrose, 26 $NaHCO_3$, 11 glucose, 10 $MgSO_4$, 2.5 KCl, 1.25 NaH_2PO_4, 0.5 $CaCl_2$, bubbled with 5% CO_2/ 95% O_2. Slices were incubated in artificial cerebrospinal fluid (aCSF) at 32°C for 30 minutes and then at room temperature until recording. aCSF contained (in mM): 123 NaCl, 26 $NaHCO_3$, 11 glucose, 3 KCl, 2 $CaCl_2$, 1.25 NaH_2PO_4, 1 $MgCl_2$, also bubbled with 5% CO_2/ 95% O_2. Neurons were visualized using differential interference contrast or DODT contrast microscopy on an upright microscope (Olympus). *Ntsr1-cre* positive neurons were identified by fluorescent visualization of cre-dependent tdTomato. We obtained somatic whole-cell patch clamp recordings using a Multiclamp 700B (Molecular Devices) amplifier and acquired with pClamp. Patch pipettes (2-5 MΩ tip resistance) were filled with the following (in mM): 130 KGluconate, 10 KCl, 10 HEPES, 10 EGTA, 2 $MgCl_2$, 2 MgATP, 0.3 Na_3GTP. All recordings were made at 32-34°C. Series resistance was compensated in all current clamp experiments and monitored throughout recordings. Recordings were discarded if Rs changed by > 25%. For spontaneous EPSC and IPSC recordings cells were held in voltage clamp at −70 mV and +10mV, respectively. In both cases patch pipettes were filled with the following (in mM): 135 Cesium Methanesulfonate, 8 NaCl, 10 HEPES, 0.3 EGTA, 5 QX314, 4 MgATP, 0.3 Na_3GTP.

Behavioral Assays

Experiments were conducted during the light cycle (8am to 8pm). Mice were habituated to investigator handling for 1-2min on three consecutive days. On the testing day, mice were transferred to experimental room and allowed to habituate for at least 45 minutes prior to testing. All behavior assays were performed on mice age P56 to P80. We were blind to the genotypes during scoring of videos.

Open-field test

An individual mouse was placed near the wall-side of 50 × 50 cm open-field arena, and the movement of the mouse was recorded by a video camera for 10 min. The recorded video file was analyzed with Any-Maze software (San Diego Instruments). Time in the center of the field (a 25 × 25 cm square) was measured. The open field arena was cleaned with 70% ethanol and wiped with paper towels between each trial.

Elevated plus maze test

An individual mouse was placed at the junction of the open and closed arms, facing the arm opposite to the experimenter, of an apparatus with two open arms without walls (30 × 5 x 0.5 cm) across from each other and perpendicular to two closed arms with walls (30 × 5 x 15 cm) with a center platform (5 × 5 cm), and at a height of 40 cm above the floor. The movement of the mouse was recorded by a video camera for 10 min. The recorded video file was analyzed with Any-Maze software and time in the open arms of the apparatus was measured. The arms of the elevated plus maze apparatus was cleaned with 70% ethanol and wiped with paper towels between each trial.

Rotarod test

The assay consisted of four trials per day over the course of 2 days with the rotarod set to accelerate from 4rpm to 45rpm over 5 minutes. The trial started once five mice were placed on the rotarod rotating at 4rpm in separate partitioned compartments. Each trial ended when a mouse fell off, made three complete revolutions while hanging on, or reached 300 s. Digital videos of the mice on the rotarod were recorded from behind. The rotarod apparatus was cleaned with 70% ethanol and wiped with paper towels between each trial.

Social interaction and novel object task

An individual mouse was allowed to habituate for 5 minutes in their home cage prior to starting the trial. A juvenile (3-4 weeks old) mouse of the same strain and sex was introduced to the home cage. After 5 minutes, the juvenile was removed from the home cage. After a 5 min break a novel object (typically a plastic test tube cap) was introduced into the home cage for five minutes. We scored videos offline, blind to genotype. We measured the number of seconds the mouse spent with its nose in direct contact with the novel object or engaged in social interaction with the juvenile (defined as sniffing, close following, or allo-grooming) in the 300 s following the time the juvenile or object was introduced into the cage. In addition, we noted any aggressive-appearing behaviors toward the juvenile, freezing, and grooming behaviors.

QUANTIFICATION AND STATISTICAL ANALYSIS

All individual data points are shown as well as mean ± SEM. All statistical analyses were performed using GraphPad Prism 7.0 software. Statistical significance was accepted at the level $p < 0.05$. We used Student's t test to compare pairs of groups if data were normally distributed (verified using Lillie test). If more than two groups were compared, we used one-way ANOVA with post hoc tests between groups corrected for multiple comparisons (Holm-Sidak or Tukey). For the ISH experiments reported in this paper n = 2 represents two biological replicates for each of the reported genes. We examined the changes in synapse numbers of n = 30 different dendrites from n = 2 animals for each genotype. Whole-cell patch clamp experiments at P21 and P56 were conducted from n = 3 different animals for each age and genotype. Lastly, behavioral analysis was conducted from n = 11/8/9, wild-type, heterozygous, homozygous animals. The specific n for each experiment as well as the post hoc test, exact F and corrected p values can be found in the Results section.

DATA AND SOFTWARE AVAILABILITY

Data and MATLAB analysis scripts are available upon request from the Lead Contact.